Frontiers of Information Technology & Electronic Engineering
www.jzus.zju.edu.cn; engineering.cae.cn; www.springerlink.com
ISSN 2095-9184 (print); ISSN 2095-9230 (online)
E-mail: jzus@zju.edu.cn

Decentralized fault-tolerant cooperative control of multiple UAVs with prescribed attitude synchronization tracking performance under directed communication topology*

Zi-quan YU[1,2,3], Zhi-xiang LIU[2], You-min ZHANG[†‡2], Yao-hong QU[1], Chun-yi SU[2]

[1]*School of Automation, Northwestern Polytechnical University, Xi'an 710129, China*

[2]*Department of Mechanical, Industrial and Aerospace Engineering, Concordia University, Montreal QC H3G 1M8, Canada*

[3]*College of Automation Engineering, Nanjing University of Aeronautics and Astronautics, Nanjing 211106, China*

[†]E-mail: ymzhang@encs.concordia.ca

Received Sept. 15, 2018; Revision accepted Mar. 20, 2019; Crosschecked May 13, 2019

Abstract: In this paper, a decentralized fault-tolerant cooperative control scheme is developed for multiple unmanned aerial vehicles (UAVs) in the presence of actuator faults and a directed communication network. To counteract in-flight actuator faults and enhance formation flight safety, neural networks (NNs) are used to approximate unknown nonlinear terms due to the inherent nonlinearities in UAV models and the actuator loss of control effectiveness faults. To further compensate for NN approximation errors and actuator bias faults, the disturbance observer (DO) technique is incorporated into the control scheme to increase the composite approximation capability. Moreover, the prediction errors, which represent the approximation qualities of the states induced by NNs and DOs to the measured states, are integrated into the developed fault-tolerant cooperative control scheme. Furthermore, prescribed performance functions are imposed on the attitude synchronization tracking errors, to guarantee the prescribed synchronization tracking performance. One of the key features of the proposed strategy is that unknown terms due to the inherent nonlinearities in UAVs and actuator faults are compensated for by the composite approximators constructed by NNs, DOs, and prediction errors. Another key feature is that the attitude synchronization tracking errors are strictly constrained within the prescribed bounds. Finally, simulation results are provided and have demonstrated the effectiveness of the proposed control scheme.

Key words: Fault-tolerant control; Decentralized control; Prescribed performance; Unmanned aerial vehicle; Neural network; Disturbance observer; Directed topology

https://doi.org/10.1631/FITEE.1800569 **CLC number:** TP273

1 Introduction

The past decade has witnessesed a great deal of research interest in cooperative control of multiple unmanned aerial vehicles (multi-UAVs), since the implementation of multi-UAVs instead of a single UAV increases system reliability and efficiency and reduces the overall cost of a mission (Waharte and Trigoni, 2010; Nigam et al., 2012; Yuan et al., 2015;

‡ Corresponding author

* Project supported by the National Natural Science Foundation of China (Nos. 61833013, 61573282, and 61473229), the Natural Science Foundation of Shaanxi Province, China (No. 2015JZ020), and the Natural Sciences and Engineering Research Council of Canada

ORCID: You-min ZHANG, http://orcid.org/0000-0002-9731-5943

Yan et al., 2017). For the reduction of communicational and computational burdens in cooperative control of multi-UAVs, the decentralized control architecture is more efficient than the centralized control frame.

Numerous results have been obtained for cooperative control of multiple vehicles in a communication network, where each vehicle can use only its individual states and neighboring vehicles' states to determine its behaviors (Ren et al., 2007; Han et al., 2015). Bayezit and Fidan (2013) proposed a decentralized cohesive motion control scheme for an autonomous formation, such that the formation can move from the initial positions to the final desired positions while maintaining the formation geometry during the motion. This method was then extended to the cases of fixed-wing UAVs and quadrotors. Liao et al. (2017) developed a cascade robust feedback control approach for formation control of multiple vertical takeoff and landing (VTOL) UAVs in a dynamic communication network, where a potential field approach was used to generate a desired velocity in the outer loop and a velocity controller was then designed to track the desired velocity in the inner loop. He et al. (2016) investigated the output-feedback formation tracking problem of multi-UAVs by integrating a state observer, a virtual structure, and a path following approach. Using a differential game approach, Lin (2014) considered a formation control problem for multi-UAVs in a communication network, and each UAV was able to exchange information with others via an information graph. Then a formation control protocol was proposed for multi-UAVs and each UAV tried to minimize its terminal formation errors, velocity errors, and control efforts. It should be stressed that most existing results on cooperative control of multi-UAVs are about the point-mass model (Lin, 2014; He et al., 2016; Xue et al., 2016), i.e., the outer loop model. Regarding the attitude model, i.e., the inner loop model, few results have been obtained, because their focuses are the position formation control, and/or nonlinearities inherent in the attitude model are strongly coupled. However, to incorporate many practical situations in research, such as actuator saturation, faults, and dead-zone, the attitude model should be considered in the cooperative control of multi-UAVs. Furthermore, investigation on the attitude synchronization tracking control of multi-UAVs can be seen as the replenishment of existing results about the point-mass UAV model.

For the formation flight of multi-UAVs, actuator faults may cause performance degradation or even lead to a chain of failing UAVs, and this may cause catastrophes (Shi et al., 2017). In the past few decades, fault-tolerant control (FTC) against actuator faults has attracted much attention, and numerous results have been reported (Zhang and Jiang, 2008; Liu et al., 2016, 2017; Wang and Zhang, 2018; Yu X et al., 2018a, 2018b; Yu Z et al., 2018). Xu et al. (2014) and Yu et al. (2016) investigated fault-tolerant cooperative control (FTCC) strategies of multi-UAVs in the leader-follower architecture. Regarding the FTCC of multi-UAVs in a decentralized communication network, little literature is available. Therefore, more investigations should be conducted to develop effective FTCC control schemes for multi-UAVs in a decentralized communication network.

The emphases of most existing results reported on an FTC of a single UAV or an FTCC of multi-UAVs are placed on how to guarantee the tracking error for converging to a bounded region or an origin, which can be seen as research handling only steady-state performance. However, to improve flight performance in the case of actuator faults, research is needed on transient performance, including overshoot and convergence rate, to achieve a safe formation flight of multi-UAVs. The prescribed performance control (PPC) proposed by Bechlioulis and Rovithakis (2008, 2010) is that using a prescribed performance function and an error transformation function, the tracking error will converge to a predefined small residual set. Moreover, the convergence rate of the tracking error will not violate the decreasing rate of the prescribed performance function. Based on the dynamic surface design architecture, an FTC scheme was proposed by Qian et al. (2016) for a single UAV by considering the transient tracking performance with the prescribed performance function. By estimating the bounds of fault uncertainties and using a PPC method, an adaptive FTC scheme was developed by Li et al. (2017) for a single hypersonic flight vehicle in the presence of elevator faults. Tracking errors were reduced to the predefined small residual set with prescribed maximum overshoots and convergence rates. To the best of our knowledge, few results on the FTCC scheme for multi-UAVs in a decentralized communication

network with prescribed attitude synchronization tracking performance have been reported.

Motivated by the aforementioned analyses, we attempt to develop a decentralized FTCC scheme for multi-UAVs with prescribed attitude synchronization tracking performance, such that all UAVs can synchronously track their attitude references in the presence of actuator faults. Specifically, to constrain the synchronization errors within the prescribed bounds, synchronization errors are first transformed into a new set of error variables by the prescribed performance functions. Then neural networks (NNs) are used to approximate unknown nonlinear terms due to the nonlinearities inherent in UAVs and the loss of control effectiveness actuator faults. Disturbance observers (DOs) are used to compensate for NN approximation errors and bias faults. Furthermore, prediction errors are incorporated into NN adaptive laws and DOs to enhance approximation abilities. Compared with other existing works, the main contributions of this study are summarized as follows: (1) The attitude synchronization tracking control of multi-UAVs is investigated in a decentralized communication network with a directed information flow rather than a centralized communication topology; (2) Compared with numerous results of FTC of a single UAV and several studies on the FTCC of multi-UAVs in a leader-follower framework, an attitude synchronization FTCC scheme is further developed for multi-UAVs in a decentralized communication network; (3) Transient fault-tolerant synchronization tracking performance is considered by incorporating the prescribed performance function.

2 Preliminaries and problem statement

2.1 Unmanned aerial vehicle model

In this study, it is assumed that there exist N UAVs in the formation team. By denoting $\Omega = \{1,\ 2,\ ...,\ N\}$ as the set of UAVs, the inertial position coordinates of the i^{th} UAV are expressed as

$$\begin{cases} \dot{x}_i = V_i \cos\gamma_i \cos\chi_i, \\ \dot{y}_i = V_i \cos\gamma_i \sin\chi_i, \\ \dot{z}_i = V_i \sin\gamma_i, \end{cases} \tag{1}$$

where $i \in \Omega$, x_i, y_i, and z_i are the positions, and V_i, γ_i, and χ_i are velocity, flight path angle (FPA), and heading angle, respectively.

The force equations are presented as

$$\begin{cases} \dot{V}_i = \dfrac{1}{m_i}(-D_i + T_i \cos\alpha_i \cos\beta_i) - g\sin\gamma_i, \\ \dot{\chi}_i = \dfrac{1}{m_i V_i \cos\gamma_i}(L_i \sin\mu_i + Y_i \cos\mu_i) \\ \qquad + \dfrac{T_i}{m_i V_i \cos\gamma_i}(\sin\alpha_i \sin\mu_i - \cos\alpha_i \sin\beta_i \cos\mu_i), \\ \dot{\gamma}_i = \dfrac{1}{m_i V_i}(L_i \cos\mu_i - Y_i \sin\mu_i) - \dfrac{g\cos\gamma_i}{V_i} \\ \qquad + \dfrac{T_i}{m_i V_i}(\cos\alpha_i \sin\beta_i \sin\mu_i + \sin\alpha_i \cos\mu_i), \end{cases} \tag{2}$$

where $i \in \Omega$, m_i and g are the mass and gravitational constant respectively, μ_i, α_i, and β_i are the bank angle, angle of attack, and sideslip angle respectively, and T_i, D_i, L_i, and Y_i are the thrust, drag, lift, and lateral forces respectively.

The attitude kinematic model is expressed as

$$\begin{cases} \dot{\alpha}_i = q_i - \tan\beta_i(p_i \cos\alpha_i + r_i \sin\alpha_i) \\ \qquad - (\dot{\chi}_i \cos\gamma_i \sin\mu_i + \dot{\gamma}_i \cos\mu_i)/\cos\beta_i, \\ \dot{\beta}_i = p_i \sin\alpha_i - r_i \cos\alpha_i + \dot{\chi}_i \cos\gamma_i \cos\mu_i - \dot{\gamma}_i \sin\mu_i, \\ \dot{\mu}_i = (p_i \cos\alpha_i + r_i \sin\alpha_i)/\cos\beta_i + \dot{\gamma}_i \cos\mu_i \tan\beta_i \\ \qquad + \dot{\chi}_i(\sin\gamma_i + \cos\gamma_i \sin\mu_i \tan\beta_i), \end{cases} \tag{3}$$

where $i \in \Omega$, and p_i, q_i, and r_i are the angular rates.

The attitude dynamic model is given as

$$\begin{cases} \dot{p}_i = (c_{i1} r_i + c_{i2} p_i) q_i + c_{i3} \mathcal{L}_i + c_{i4} \mathcal{N}_i, \\ \dot{q}_i = c_{i5} p_i r_i - c_{i6}(p_i^2 - r_i^2) + c_{i7} \mathcal{M}_i, \\ \dot{r}_i = (c_{i8} p_i - c_{i2} r_i) q_i + c_{i4} \mathcal{L}_i + c_{i9} \mathcal{N}_i, \end{cases} \tag{4}$$

where $i \in \Omega$, and $\mathcal{L}_i$, $\mathcal{M}_i$, and $\mathcal{N}_i$ are roll, pitch, and yaw moments, respectively.

The forces T_i, D_i, L_i, and Y_i and the aerodynamic moments $\mathcal{L}_i$, $\mathcal{M}_i$, and $\mathcal{N}_i$ are expressed as

$$\begin{cases} T_i = T_{i\max} \delta_{T_i},\ D_i = Q_i s_i C_{iD}, \\ L_i = Q_i s_i C_{iL},\ Y_i = Q_i s_i C_{iY}, \\ \mathcal{L}_i = Q_i s_i b_i C_{i\mathcal{L}},\ \mathcal{M}_i = Q_i s_i c_i C_{i\mathcal{M}}, \\ \mathcal{N}_i = Q_i s_i b_i C_{i\mathcal{N}}, \end{cases} \tag{5}$$

where $Q_i = \rho V_i^2/2$ is the dynamic pressure, s_i, b_i, and c_i represent the wing area, wing span, and mean aerodynamic chord respectively, and $T_{i\max}$ and δ_{T_i} are the maximum thrust and instantaneous thrust

throttle setting, respectively. C_{iL}, C_{iD}, C_{iY}, $C_{i\mathcal{L}}$, $C_{i\mathcal{M}}$, and $C_{i\mathcal{N}}$ are given by

$$\begin{cases} C_{iL} = C_{iL0} + C_{iL\alpha}\alpha_i, \\ C_{iD} = C_{iD0} + C_{iD\alpha}\alpha_i + C_{iD\alpha^2}\alpha_i^2, \\ C_{iY} = C_{iY0} + C_{iY\beta}\beta_i, \end{cases} \tag{6}$$

$$\begin{cases} C_{i\mathcal{L}} = C_{i\mathcal{L}0} + C_{i\mathcal{L}\beta}\beta_i + C_{i\mathcal{L}\delta_{\rm a}}\delta_{i\rm a} + C_{i\mathcal{L}\delta_{\rm r}}\delta_{i\rm r} \\ \qquad + \dfrac{C_{i\mathcal{L}p}b_i p_i}{2V_i} + \dfrac{C_{i\mathcal{L}r}b_i r_i}{2V_i}, \\ C_{i\mathcal{M}} = C_{i\mathcal{M}0} + C_{i\mathcal{M}\alpha}\alpha_i + C_{i\mathcal{M}\delta_{\rm e}}\delta_{i\rm e} + \dfrac{C_{i\mathcal{M}q}c_i q_i}{2V_i}, \\ C_{i\mathcal{N}} = C_{i\mathcal{N}0} + C_{i\mathcal{N}\beta}\beta_i + C_{i\mathcal{N}\delta_{\rm a}}\delta_{i\rm a} + C_{i\mathcal{N}\delta_{\rm r}}\delta_{i\rm r} \\ \qquad + \dfrac{C_{i\mathcal{N}p}b_i p_i}{2V_i} + \dfrac{C_{i\mathcal{N}r}b_i r_i}{2V_i}, \end{cases} \tag{7}$$

where $\delta_{i\rm a}$, $\delta_{i\rm e}$, and $\delta_{i\rm r}$ are aileron, elevator, and rudder deflections, respectively, and C_{iL0}, $C_{iL\alpha}$, C_{iD0}, $C_{iD\alpha}$, $C_{iD\alpha^2}$, C_{iY0}, $C_{iY\beta}$, $C_{i\mathcal{L}0}$, $C_{i\mathcal{L}\beta}$, $C_{i\mathcal{L}\delta_{\rm a}}$, $C_{i\mathcal{L}\delta_{\rm r}}$, $C_{i\mathcal{L}p}$, $C_{i\mathcal{L}r}$, $C_{i\mathcal{M}0}$, $C_{i\mathcal{M}\alpha}$, $C_{i\mathcal{M}\delta_{\rm e}}$, $C_{i\mathcal{M}q}$, $C_{i\mathcal{N}0}$, $C_{i\mathcal{N}\beta}$, $C_{i\mathcal{N}\delta_{\rm a}}$, $C_{i\mathcal{N}\delta_{\rm r}}$, $C_{i\mathcal{N}p}$, and $C_{i\mathcal{N}r}$ are aerodynamic coefficients. Definitions of inertial terms c_{ij} (j=1, 2, ..., 9) in Eq. (4) are referred to Yu Z et al. (2018).

Defining $\boldsymbol{x}_{i1} = [\mu_i,\ \alpha_i,\ \beta_i]^{\rm T}$, $\boldsymbol{x}_{i2} = [p_i,\ q_i,\ r_i]^{\rm T}$, and $\boldsymbol{u}_i = [\delta_{i\rm a},\ \delta_{i\rm e},\ \delta_{i\rm r}]^{\rm T}$, the attitude model can be formulated as

$$\dot{\boldsymbol{x}}_{i1} = \boldsymbol{f}_{i1} + \boldsymbol{g}_{i1}\boldsymbol{x}_{i2}, \tag{8}$$

$$\dot{\boldsymbol{x}}_{i2} = \boldsymbol{f}_{i2} + \boldsymbol{g}_{i2}\boldsymbol{u}_i, \tag{9}$$

where $\boldsymbol{f}_{i1}$, $\boldsymbol{f}_{i2}$, $\boldsymbol{g}_{i1}$, and $\boldsymbol{g}_{i2}$ are expressed at the top of the next page, with f_{i21}, f_{i22}, f_{i23}, g_{i211}, g_{i213}, g_{i222}, g_{i231}, and g_{i233} also being expressed at the top of the next page.

Assumption 1 The control gain function $\boldsymbol{g}_{i2}$ can be written as a known part $\boldsymbol{g}_{i2N}$ and an unknown part $\Delta\boldsymbol{g}_{i2}$.

Remark 1 From the expression of $\boldsymbol{g}_{i2}$, it is observed that $\boldsymbol{g}_{i2}$ depends on the aerodynamic coefficients $C_{i\mathcal{L}\delta_{\rm a}}$, $C_{i\mathcal{N}\delta_{\rm a}}$, $C_{i\mathcal{L}\delta_{\rm r}}$, $C_{i\mathcal{N}\delta_{\rm r}}$, and $C_{i\mathcal{M}\delta_{\rm e}}$. In controller design, rough aerodynamic coefficient values can be obtained by simple wind tunnel test or software calculation. Therefore, it is reasonable to assume $\boldsymbol{g}_{i2} = \boldsymbol{g}_{i2N} + \Delta\boldsymbol{g}_{i2}$ in the controller design. In the attitude dynamic models (8) and (9), $\boldsymbol{f}_{i1}$ and $\boldsymbol{f}_{i2}$ are unknown nonlinear functions.

2.2 Actuator fault model

In practical engineering applications, actuator faults may degrade system performance or even lead to system instability if faults are not handled in a timely manner. Actuator loss of control effectiveness and bias faults are often encountered by UAVs in formation flying. To facilitate the fault-tolerant controller design, the actuator fault model is first given by

$$\boldsymbol{u}_i = \boldsymbol{\rho}_i\boldsymbol{u}_{i0} + \boldsymbol{u}_{if}, \tag{10}$$

where $\boldsymbol{u}_i = [\delta_{i\rm a},\ \delta_{i\rm e},\ \delta_{i\rm r}]^{\rm T}$ is an applied signal, $\boldsymbol{u}_{i0} = [\delta_{i\rm a0},\ \delta_{i\rm e0},\ \delta_{i\rm r0}]^{\rm T}$ is a control signal commanded by a controller, $\boldsymbol{\rho}_i = {\rm diag}(\rho_{i1},\ \rho_{i2},\ \rho_{i3})$ represents a remaining control effectiveness factor, and $\boldsymbol{u}_{if} = [u_{if1},\ u_{if2},\ u_{if3}]^{\rm T}$ denotes a bounded bias fault.

By applying the actuator fault model (10) into model (9), the attitude dynamic model in the presence of actuator faults is formulated as

$$\dot{\boldsymbol{x}}_{i2} = \boldsymbol{F}_{i2} + \boldsymbol{g}_{i2N}\boldsymbol{u}_{i0} + \boldsymbol{d}_i, \tag{11}$$

where $\boldsymbol{F}_{i2} = \boldsymbol{f}_{i2} + \boldsymbol{g}_{i2N}\boldsymbol{\rho}_i\boldsymbol{u}_{i0} + \Delta\boldsymbol{g}_{i2}\boldsymbol{\rho}_i\boldsymbol{u}_{i0} - \boldsymbol{g}_{i2N}\boldsymbol{u}_{i0}$ and $\boldsymbol{d}_i = (\boldsymbol{g}_{i2N} + \Delta\boldsymbol{g}_{i2})\boldsymbol{u}_{if}$.

Therefore, the attitude model in the presence of actuator faults is given by

$$\dot{\boldsymbol{x}}_{i1} = \boldsymbol{f}_{i1} + \boldsymbol{g}_{i1}\boldsymbol{x}_{i2}, \tag{12}$$

$$\dot{\boldsymbol{x}}_{i2} = \boldsymbol{F}_{i2} + \boldsymbol{g}_{i2N}\boldsymbol{u}_{i0} + \boldsymbol{d}_i. \tag{13}$$

It should be noted that the unknown nonlinear function $\boldsymbol{F}_{i2}$ involves a control input signal $\boldsymbol{u}_{i0}$. Algebraic loops will be introduced into the controller design if the radial basis function neural network (RBFNN) is employed to approximate the nonlinear function, since the input signal $\boldsymbol{u}_{i0}$ is directly fed into the Gaussian function of the RBFNN. To break the algebraic loop, a Butterworth low-pass filter is introduced as

$$\boldsymbol{u}_{i0f} = \boldsymbol{B}_i(s)\boldsymbol{u}_{i0} \approx \boldsymbol{u}_{i0}, \tag{14}$$

where $\boldsymbol{B}_i(s)$ is a Butterworth low-pass filter, and $\boldsymbol{u}_{i0f}$ is the filtered signal.

Therefore, one has

$$\boldsymbol{\varepsilon}_i = \boldsymbol{F}_{i2}(\boldsymbol{u}_{i0}) - \boldsymbol{F}_{i2b}(\boldsymbol{u}_{i0f}), \tag{15}$$

where $\boldsymbol{\varepsilon}_i$ is a bounded filter error (Zou et al., 2008).

$$
\begin{aligned}
\boldsymbol{f}_{i1} =& \begin{bmatrix} 0 & \sin\gamma_i + \cos\gamma_i\sin\mu_i\tan\beta_i & \cos\mu_i\tan\beta_i \\ 0 & -\cos\gamma_i\sin\mu_i/\cos\beta_i & -\cos\mu_i/\cos\beta_i \\ 0 & \cos\gamma_i\cos\mu_i & -\sin\mu_i \end{bmatrix} \cdot \\
& \begin{bmatrix} \dfrac{-D_i + T_i\cos\alpha_i\cos\beta_i}{m_i} - g\sin\gamma_i \\ \dfrac{L_i\sin\mu_i + Y_i\cos\mu_i + T_i(\sin\alpha_i\sin\mu_i - \cos\alpha_i\sin\beta_i\cos\mu_i)}{m_i V_i\cos\gamma_i} \\ \dfrac{L_i\cos\mu_i - Y_i\sin\mu_i - m_i g\cos\gamma_i + T_i(\cos\alpha_i\sin\beta_i\sin\mu_i + \sin\alpha_i\cos\mu_i)}{m_i V_i} \end{bmatrix}, \\
\boldsymbol{f}_{i2} =& [f_{i21}, f_{i22}, f_{i23}]^{\mathrm{T}}, \\
\boldsymbol{g}_{i1} =& \begin{bmatrix} \cos\alpha_i/\cos\beta_i & 0 & \sin\alpha_i/\cos\beta_i \\ -\cos\alpha_i\tan\beta_i & 1 & -\sin\alpha_i\tan\beta_i \\ \sin\alpha_i & 0 & -\cos\alpha_i \end{bmatrix}, \\
\boldsymbol{g}_{i2} =& \begin{bmatrix} g_{i211} & 0 & g_{i213} \\ 0 & g_{i222} & 0 \\ g_{i231} & 0 & g_{i233} \end{bmatrix},
\end{aligned}
$$

$$
\begin{aligned}
f_{i21} =& c_{i1}q_i r_i + c_{i2}p_i q_i + c_{i3}Q_i s_i b_i(C_{i\mathcal{L}0} + C_{i\mathcal{L}\beta}\beta_i + C_{i\mathcal{L}p}b_i p_i/2V_i + C_{i\mathcal{L}r}b_i r_i/2V_i) \\
& + C_{i4}Q_i s_i b_i(C_{i\mathcal{N}0} + C_{i\mathcal{N}\beta}\beta_i + C_{i\mathcal{N}p}b_i p_i/2V_i + C_{i\mathcal{N}r}b_i r_i/2V_i), \\
f_{i22} =& c_{i5}p_i r_i - c_{i6}(p_i^2 - r_i^2) + c_{i7}Q_i s_i c_i(C_{i\mathcal{M}0} + C_{i\mathcal{M}\alpha}\alpha_i + C_{i\mathcal{M}q}c_i q_i/2V_i), \\
f_{i23} =& c_{i8}p_i q_i - c_{i2}q_i r_i + c_{i4}Q_i s_i b_i(C_{i\mathcal{L}0} + C_{i\mathcal{L}\beta}\beta_i + C_{i\mathcal{L}p}b_i p_i/2V_i + C_{i\mathcal{L}r}b_i r_i/2V_i) \\
& + c_{i9}Q_i s_i b_i(C_{i\mathcal{N}0} + C_{i\mathcal{N}\beta}\beta_i + C_{i\mathcal{N}p}b_i p_i/2V_i + C_{i\mathcal{N}r}b_i r_i/2V_i), \\
g_{i211} =& c_{i3}Q_i s_i b_i C_{i\mathcal{L}\delta_{\mathrm{a}}} + c_{i4}Q_i s_i b_i C_{i\mathcal{N}\delta_{\mathrm{a}}}, \\
g_{i213} =& c_{i3}Q_i s_i b_i C_{i\mathcal{L}\delta_{\mathrm{r}}} + c_{i4}Q_i s_i b_i C_{i\mathcal{N}\delta_{\mathrm{r}}}, \\
g_{i222} =& c_{i7}Q_i s_i c_i C_{i\mathcal{M}\delta_{\mathrm{e}}}, \\
g_{i231} =& c_{i4}Q_i s_i b_i C_{i\mathcal{L}\delta_{\mathrm{a}}} + c_{i9}QS_i b_i C_{i\mathcal{N}\delta_{\mathrm{a}}}, \\
g_{i233} =& c_{i4}Q_i s_i b_i C_{i\mathcal{L}\delta_{\mathrm{r}}} + c_{i9}Q_i s_i b_i C_{i\mathcal{N}\delta_{\mathrm{r}}}.
\end{aligned}
$$

Considering the filter error $\boldsymbol{\varepsilon}_i$, model (13) can be further transformed to

$$\dot{\boldsymbol{x}}_{i2} = \boldsymbol{F}_{i2b} + \boldsymbol{g}_{i2N}\boldsymbol{u}_{i0} + \boldsymbol{d}_i + \boldsymbol{\varepsilon}_i. \tag{16}$$

Based on the control-oriented attitude models (12) and (16), a decentralized FTCC scheme will be developed. Since the control scheme is to be developed for multi-UAVs in a decentralized communication network, the basic graph theory will be given in the subsequent subsection.

2.3 Basic graph theory

Assume that the information exchange of N UAVs is modeled by a weighted-directed graph $\mathcal{G} = (\mathcal{V},\ \mathcal{E},\ \boldsymbol{\mathcal{A}})$, where $\mathcal{V} = \{v_1,\ v_2,\ ...,\ v_N\}$ is a set of nodes, $\mathcal{E} \subseteq \mathcal{V} \times \mathcal{V}$ is a set of edges, and $\boldsymbol{\mathcal{A}} = [a_{ij}] \in \mathbb{R}^{N\times N}$ is a weighted adjacency matrix of graph $\mathcal{G}$. Node v_j can access information from node v_i if $(v_i,\ v_j) \in \mathcal{E}$. The set of neighbors of node v_i is denoted as $N_i = \{v_j \in \mathcal{V} | (v_j,\ v_i) \in \mathcal{E}\}$. A directed path from v_i to v_j is a sequence of edges of the forms $(v_i,\ v_{l_1})$, $(v_{l_1},\ v_{l_2})$, ..., and $(v_{l_k},\ v_j)$, where $v_{l_n} \in \mathcal{V}$ for $1 \le l_n \le l_k$. The elements of $\boldsymbol{\mathcal{A}}$ are defined as $a_{ij} > 0$ if $(v_j, v_i) \in \mathcal{E}$; otherwise, $a_{ij} = 0$. The Laplacian matrix $\boldsymbol{\mathcal{L}} = [l_{ij}] \in \mathbb{R}^{N\times N}$ associated with graph $\mathcal{G}$ is defined as $l_{ij} = \sum_{k=1}^{N} a_{ik}$ if $i = j$; otherwise, $l_{ij} = -a_{ij}$.

Lemma 1 For a weighted-directed graph $\mathcal{G}$ with

N nodes, all eigenvalues of the weighted Laplacian $\boldsymbol{\mathcal{L}}$ have a nonnegative real part (Wu et al., 2011).

Lemma 2 Suppose $\boldsymbol{X} \in \mathbb{R}^{m\times m}$ and $\boldsymbol{Y} \in \mathbb{R}^{n\times n}$, and let λ_{11}, λ_{12}, ..., and λ_{1m} be the eigenvalues of $\boldsymbol{X}$ and λ_{21}, λ_{22}, ..., and λ_{2m} be the eigenvalues of $\boldsymbol{Y}$. Then the eigenvalues of $\boldsymbol{X}\otimes\boldsymbol{Y}$ are $\lambda_{1i}\lambda_{2j}$, $i = 1, 2, ..., m$, $j = 1, 2, ..., n$, where "$\otimes$" denotes the Kronecker product (Wu et al., 2011).

2.4 Control objective

The objective of this study is to design a set of decentralized FTCC laws for a group of UAVs in the presence of actuator faults and directed communication network, such that all attitudes of multi-UAVs can track their attitude references with prescribed synchronization tracking performance.

3 Main results

In this section, a decentralized FTCC scheme is developed with the integration of PPC, NNs, and DOs. Auxiliary systems are used in the proposed control scheme to compensate for the errors induced by the first-order filter and actuator saturation.

3.1 Performance function and error transformation

By defining the desired attitude reference of the i^{th} UAV as $\boldsymbol{x}_{i1\text{d}} = [\mu_{i\text{d}}, \alpha_{i\text{d}}, \beta_{i\text{d}}]^{\text{T}}$, the individual attitude tracking error of each UAV is denoted as $\tilde{\boldsymbol{x}}_{i1} = \boldsymbol{x}_{i1} - \boldsymbol{x}_{i1\text{d}}$. Define the attitude synchronization tracking error as

$$\boldsymbol{e}_{i1} = \lambda_1\tilde{\boldsymbol{x}}_{i1} + \lambda_2\sum_{j=1}^{N_i} a_{ij}(\tilde{\boldsymbol{x}}_{i1} - \tilde{\boldsymbol{x}}_{j1}), \tag{17}$$

where $\boldsymbol{e}_{i1} = [e_{i11}, e_{i12}, e_{i13}]^{\text{T}}$, and λ_1 and λ_2 are positive constants which are determined by the controller designer to regulate the convergence rate of the state trajectory. Note that λ_1 is related to the attitude tracking of the i^{th} UAV, i.e., the station-keeping behavior, and λ_2 and a_{ij} are associated with the attitude synchronization between the i^{th} and j^{th} UAVs, i.e., the formation-keeping behavior.

Using the Kronecker product, one has

$$\boldsymbol{e}_1 = [(\lambda_1\boldsymbol{I}_N + \lambda_2\boldsymbol{\mathcal{L}})\otimes\boldsymbol{I}_3]\tilde{\boldsymbol{x}}_1, \tag{18}$$

where $\boldsymbol{e}_1 = [\boldsymbol{e}_{11}^{\text{T}}, \boldsymbol{e}_{21}^{\text{T}}, ..., \boldsymbol{e}_{N1}^{\text{T}}]^{\text{T}}$, $\tilde{\boldsymbol{x}}_1 = [\tilde{\boldsymbol{x}}_{11}^{\text{T}}, \tilde{\boldsymbol{x}}_{21}^{\text{T}}, ..., \tilde{\boldsymbol{x}}_{N1}^{\text{T}}]^{\text{T}}$, and $\boldsymbol{I}_N$ and $\boldsymbol{I}_3$ are identity matrices with appropriate dimensions.

In the view of Lemmas 1 and 2, one can conclude that $(\lambda_1\boldsymbol{I}_N + \lambda_2\boldsymbol{\mathcal{L}})\otimes\boldsymbol{I}_3$ has a full rank. Therefore, it follows that $\tilde{\boldsymbol{x}}_1 \to \boldsymbol{0}$ when $\boldsymbol{e}_1 \to \boldsymbol{0}$.

A new set of error variables is introduced to achieve the prescribed transient and steady performances, such that the fault-tolerant capability against actuator faults can be guaranteed. FTCC with prescribed performance means that the attitude synchronization tracking errors strictly evolve within the predefined residual set and that the convergence rates cannot violate the predefined values. PPC can be guaranteed if the following condition is always satisfied:

$$-\underline{k}_{i1\nu}\varepsilon_{i1\nu} \le e_{i1\nu} \le \overline{k}_{i1\nu}\varepsilon_{i1\nu}, \forall t \ge 0, \tag{19}$$

where $i \in \Omega$, $\nu = 1, 2, 3$, $\underline{k}_{i1\nu}$ and $\overline{k}_{i1\nu}$ are positive design parameters, and $\varepsilon_{i1\nu}$ is a strictly decreasing smooth function which is chosen as $\varepsilon_{i1\nu} = (\varepsilon_{i1\nu0} - \varepsilon_{i1\nu\infty})\text{e}^{-\iota_{i1\nu}t} + \varepsilon_{i1\nu\infty}$ with $\varepsilon_{i1\nu\infty}$ being the maximum allowable value of $e_{i1\nu}$ at the steady state and $\varepsilon_{i1\nu0}$ being the initial value of $\varepsilon_{i1\nu}$. Note that $\varepsilon_{i1\nu0}$, $\varepsilon_{i1\nu\infty}$, and $\iota_{i1\nu}$ are positive constants which should be chosen to satisfy $-\underline{k}_{i1\nu}\varepsilon_{i1\nu0} \le e_{i1\nu}(0) \le \overline{k}_{i1\nu}\varepsilon_{i1\nu0}$, where $-\underline{k}_{i1\nu}\varepsilon_{i1\nu}$ and $\overline{k}_{i1\nu}\varepsilon_{i1\nu}$ are allowable lower boundary of the undershoot and upper boundary of the overshoot of $e_{i1\nu}$, respectively. The allowable steady-state value of $e_{i1\nu}$ is in the region of $[-\underline{k}_{i1\nu}\varepsilon_{i1\nu\infty}, \overline{k}_{i1\nu}\varepsilon_{i1\nu\infty}]$.

To use inequality (19) for the decentralized FTCC scheme design, inequality (19) is transformed to

$$e_{i1\nu} = \varepsilon_{i1\nu}\Theta(E_{i1\nu}), \tag{20}$$

where $\Theta(\cdot)$ is a smooth and strictly increasing function with the following properties:

$$\begin{cases} \Theta(0) = 0, \\ -\underline{k}_{i1\nu} \le \Theta(E_{i1\nu}) \le \overline{k}_{i1\nu}, \\ \lim_{E_{i1\nu}\to+\infty}\Theta(E_{i1\nu}) = \overline{k}_{i1\nu}, \\ \lim_{E_{i1\nu}\to-\infty}\Theta(E_{i1\nu}) = -\underline{k}_{i1\nu}. \end{cases} \tag{21}$$

Using the error transformation (Eq. (20)), the controller design for the synchronized tracking error $e_{i1\nu}$ with prescribed performance can be converted to the control scheme design with a uniformly ultimately bounded error $E_{i1\nu}$.

In this study, $\Theta(E_{i1\nu})$ is chosen as

$$\Theta(E_{i1\nu}) = \frac{\overline{k}_{i1\nu}\text{e}^{E_{i1\nu}+\kappa_{i1\nu}} - \underline{k}_{i1\nu}\text{e}^{-E_{i1\nu}-\kappa_{i1\nu}}}{\text{e}^{E_{i1\nu}+\kappa_{i1\nu}} + \text{e}^{-E_{i1\nu}-\kappa_{i1\nu}}}, \tag{22}$$

where $\kappa_{i1\nu}=\frac{1}{2}\ln\frac{\overline{k}_{i1\nu}}{\underline{k}_{i1\nu}}$.

Combining Eqs. (20) and (22) yields

$$\begin{aligned}E_{i1\nu}=&\Theta^{-1}\frac{e_{i1\nu}}{\varepsilon_{i1\nu}}\\=&\frac{1}{2}\ln\frac{\overline{k}_{i1\nu}\underline{k}_{i1\nu}+\overline{k}_{i1\nu}\sigma_{i1\nu}}{\overline{k}_{i1\nu}\underline{k}_{i1\nu}-\underline{k}_{i1\nu}\sigma_{i1\nu}},\end{aligned}\tag{23}$$

where $\sigma_{i1\nu}=e_{i1\nu}/\varepsilon_{i1\nu}$.

Taking the time derivative of Eq. (23) yields

$$\begin{aligned}\dot{E}_{i1\nu}=&\frac{1}{2\varepsilon_{i1\nu}}\left(\frac{1}{\underline{k}_{i1\nu}+\sigma_{i1\nu}}+\frac{1}{\overline{k}_{i1\nu}-\sigma_{i1\nu}}\right)\\&\cdot\left(\dot{e}_{i1\nu}-\frac{e_{i1\nu}\dot{\varepsilon}_{i1\nu}}{\varepsilon_{i1\nu}}\right)\\=&\eta_{i1\nu}\left(\dot{e}_{i1\nu}-\frac{e_{i1\nu}\dot{\varepsilon}_{i1\nu}}{\varepsilon_{i1\nu}}\right),\end{aligned}\tag{24}$$

where $\eta_{i1\nu}=\frac{1}{2\varepsilon_{i1\nu}}[\frac{1}{\underline{k}_{i1\nu}+\sigma_{i1\nu}}+\frac{1}{\overline{k}_{i1\nu}-\sigma_{i1\nu}}]$.

Then the matrix form of Eq. (24) associated with the i^{th} UAV is given by

$$\dot{\boldsymbol{E}}_{i1}=\boldsymbol{\eta}_{i1}(\dot{\boldsymbol{e}}_{i1}-\boldsymbol{\varepsilon}_{i1}^{-1}\dot{\boldsymbol{\varepsilon}}_{i1}\boldsymbol{e}_{i1}),\tag{25}$$

where $\boldsymbol{E}_{i1}=[E_{i11},\ E_{i12},\ E_{i13}]^{\mathrm{T}}$, $\boldsymbol{\varepsilon}_{i1}=\mathrm{diag}(\varepsilon_{i11},\ \varepsilon_{i12},\ \varepsilon_{i13})$, and $\boldsymbol{\eta}_{i1}=\mathrm{diag}(\eta_{i11},\ \eta_{i12},\ \eta_{i13})$.

3.2 Decentralized FTCC with prescribed attitude synchronization tracking performance

Based on the transformed error variable (Eq. (23)), the attitude synchronization tracking controller with prescribed performance is developed with the integration of NNs and DOs. In the view of model (12) and error (17), Eq. (25) can be derived as

$$\begin{aligned}\dot{\boldsymbol{E}}_{i1}=&\boldsymbol{\eta}_{i1}(\dot{\boldsymbol{e}}_{i1}-\boldsymbol{\varepsilon}_{i1}^{-1}\dot{\boldsymbol{\varepsilon}}_{i1}\boldsymbol{e}_{i1})\\=&\boldsymbol{\eta}_{i1}\left([\phi_i\dot{\tilde{\boldsymbol{x}}}_{i1}-\lambda_2\sum_{j=1}^{N_i}a_{ij}\dot{\tilde{\boldsymbol{x}}}_{j1}-\boldsymbol{\varepsilon}_{i1}^{-1}\dot{\boldsymbol{\varepsilon}}_{i1}\boldsymbol{e}_{i1}\right)\\=&\boldsymbol{\eta}_{i1}\Bigg[\phi_i\left(\boldsymbol{f}_{i1}+\boldsymbol{g}_{i1}\boldsymbol{x}_{i2}-\dot{\boldsymbol{x}}_{i1\mathrm{d}}\right)-\lambda_2\sum_{j=1}^{N_i}a_{ij}\dot{\tilde{\boldsymbol{x}}}_{j1}\\&-\boldsymbol{\varepsilon}_{i1}^{-1}\dot{\boldsymbol{\varepsilon}}_{i1}\boldsymbol{e}_{i1}\Bigg],\end{aligned}\tag{26}$$

where $\phi_i=\lambda_1+\lambda_2\sum_{j=1}^{N_i}a_{ij}$.

Using an RBFNN to approximate $\Gamma_1\boldsymbol{f}_{i1}$ with Γ_1 being a positive design parameter, one has

$$\begin{aligned}\dot{\boldsymbol{E}}_{i1}=&\boldsymbol{\eta}_{i1}\Bigg[\phi_i\left(\Gamma_1^{-1}\boldsymbol{W}_{i1}^{*\mathrm{T}}\boldsymbol{\varphi}_{i1}+\boldsymbol{g}_{i1}\boldsymbol{x}_{i2}+\boldsymbol{D}_{i1}-\dot{\boldsymbol{x}}_{i1\mathrm{d}}\right)\\&-\lambda_2\sum_{j=1}^{N_i}a_{ij}\dot{\tilde{\boldsymbol{x}}}_{j1}-\boldsymbol{\varepsilon}_{i1}^{-1}\dot{\boldsymbol{\varepsilon}}_{i1}\boldsymbol{e}_{i1}\Bigg],\end{aligned}\tag{27}$$

where $\boldsymbol{W}_{i1}^{*}$ is an optimal weight matrix, $\boldsymbol{\varphi}_{i1}$ is a Gaussian function vector, $\boldsymbol{D}_{i1}=\Gamma_1^{-1}\boldsymbol{\xi}_{i1}$, and $\boldsymbol{\xi}_{i1}$ is a bounded RBFNN approximation error.

Assumption 2 Disturbance $\boldsymbol{D}_{i1}$ is unknown but has a bounded variation, and there exists an unknown positive constant $\bar{D}_{i1m}$ such that

$$\dot{\boldsymbol{D}}_{i1}^{\mathrm{T}}\dot{\boldsymbol{D}}_{i1}\le\bar{D}_{i1m}.\tag{28}$$

To move on, the prediction error is introduced as

$$\begin{cases}\boldsymbol{\Upsilon}_{i1}=\boldsymbol{x}_{i1}-\hat{\boldsymbol{x}}_{i1},\\\dot{\hat{\boldsymbol{x}}}_{i1}=\Gamma_1^{-1}\hat{\boldsymbol{W}}_{i1}^{*\mathrm{T}}\boldsymbol{\varphi}_{i1}+\boldsymbol{g}_{i1}\boldsymbol{x}_{i2}+\hat{\boldsymbol{D}}_{i1}+k_1\boldsymbol{\Upsilon}_{i1},\end{cases}\tag{29}$$

where $\hat{\boldsymbol{W}}_{i1}^{*}$ and $\hat{\boldsymbol{D}}_{i1}$ are estimations of $\boldsymbol{W}_{i1}^{*}$ and $\boldsymbol{D}_{i1}$, respectively, and k_1 is a positive design parameter.

Using the prediction error (29), the DO is designed as

$$\begin{cases}\hat{\boldsymbol{D}}_{i1}=\boldsymbol{\pi}_{i1}+k_2\boldsymbol{x}_{i1},\\\dot{\boldsymbol{\pi}}_{i1}=-k_2\boldsymbol{\pi}_{i1}+\boldsymbol{\phi}_i\boldsymbol{\eta}_{i1}\boldsymbol{E}_{i1}-k_2\Big[\Gamma_1^{-1}\hat{\boldsymbol{W}}_{i1}^{*\mathrm{T}}\boldsymbol{\varphi}_{i1}\\\qquad\qquad+\boldsymbol{g}_{i1}\boldsymbol{x}_{i2}+k_2\boldsymbol{x}_{i1}-k_2^{-1}(k_3\phi_i\boldsymbol{\Upsilon}_{i1}+\boldsymbol{E}_{i1})\Big],\end{cases}\tag{30}$$

where k_2 and k_3 are positive design parameters.

Taking the time derivative of Eq. (30) yields

$$\begin{aligned}\dot{\hat{\boldsymbol{D}}}_{i1}=&k_2\tilde{\boldsymbol{D}}_{i1}+k_2\Gamma_1^{-1}\tilde{\boldsymbol{W}}_{i1}^{*\mathrm{T}}\boldsymbol{\varphi}_{i1}\\&+k_3\phi_i\boldsymbol{\Upsilon}_{i1}+\boldsymbol{E}_{i1}+\phi_i\boldsymbol{\eta}_{i1}\boldsymbol{E}_{i1},\end{aligned}\tag{31}$$

where $\tilde{\boldsymbol{W}}_{i1}^{*}=\boldsymbol{W}_{i1}^{*}-\hat{\boldsymbol{W}}_{i1}^{*}$ and $\tilde{\boldsymbol{D}}_{i1}=\boldsymbol{D}_{i1}-\hat{\boldsymbol{D}}_{i1}$ are estimation errors.

Taking the time derivative of $\tilde{\boldsymbol{D}}_{i1}$ yields

$$\begin{aligned}\dot{\tilde{\boldsymbol{D}}}_{i1}=&\dot{\boldsymbol{D}}_{i1}-k_2\tilde{\boldsymbol{D}}_{i1}-k_2\Gamma_1^{-1}\tilde{\boldsymbol{W}}_{i1}^{*\mathrm{T}}\boldsymbol{\varphi}_{i1}\\&-k_3\phi_i\boldsymbol{\Upsilon}_{i1}-\boldsymbol{E}_{i1}-\phi_i\boldsymbol{\eta}_{i1}\boldsymbol{E}_{i1}.\end{aligned}\tag{32}$$

Design the intermittent control signal and adaptive law as

$$\begin{aligned}\bar{\boldsymbol{x}}_{i2\mathrm{d}}=&(\phi_i\boldsymbol{g}_{i1})^{-1}(-\phi_i\Gamma_1^{-1}\hat{\boldsymbol{W}}_{i1}^{*\mathrm{T}}\boldsymbol{\varphi}_{i1}-\phi_i\hat{\boldsymbol{D}}_{i1}\\&+\phi_i\dot{\boldsymbol{x}}_{i1\mathrm{d}}+\boldsymbol{\varepsilon}_{i1}^{-1}\dot{\boldsymbol{\varepsilon}}_{i1}\boldsymbol{e}_{i1}-\boldsymbol{\eta}_{i1}^{-1}\boldsymbol{K}_4\boldsymbol{E}_{i1}\\&+k_5\boldsymbol{\mu}_{i1}+\lambda_2\sum_{j=1}^{N_i}a_{ij}\dot{\tilde{\boldsymbol{x}}}_{j1}),\end{aligned}\tag{33}$$

$$\dot{\hat{\boldsymbol{W}}}_{i1}^{*}=k_6\Big[\boldsymbol{\varphi}_{i1}\phi_i\Gamma_1^{-1}(\boldsymbol{\eta}_{i1}^{\mathrm{T}}\boldsymbol{E}_{i1}+k_3\boldsymbol{\Upsilon}_{i1})^{\mathrm{T}}-k_7\hat{\boldsymbol{W}}_{i1}^{*}\Big],\tag{34}$$

where $\boldsymbol{K}_4$ is a diagonal matrix with positive elements, k_5 a positive parameter, $\boldsymbol{\mu}_{i1}$ an auxiliary signal to be designed later, and k_6 and k_7 positive design parameters.

In this study, a dynamic surface control technique is used to facilitate the controller design, which uses the first-order filter technique to obtain the virtual control signal $\boldsymbol{x}_{i2\mathrm{d}}$ and its time derivative. The first-order filter is given by

$$\tau_i\dot{\boldsymbol{x}}_{i2\mathrm{d}}+\boldsymbol{x}_{i2\mathrm{d}}=\bar{\boldsymbol{x}}_{i2\mathrm{d}},\ \boldsymbol{x}_{i2\mathrm{d}}(0)=\bar{\boldsymbol{x}}_{i2\mathrm{d}}(0), \tag{35}$$

where τ_i is a positive design parameter, and $\boldsymbol{x}_{i2\mathrm{d}}$ is a virtual control signal and the corresponding time derivative can be calculated as $\dot{\boldsymbol{x}}_{i2\mathrm{d}}=(\bar{\boldsymbol{x}}_{i2\mathrm{d}}-\boldsymbol{x}_{i2\mathrm{d}})/\tau_i$.

To compensate for the filter error $\boldsymbol{\zeta}_{i1}=\boldsymbol{x}_{i2\mathrm{d}}-\bar{\boldsymbol{x}}_{i2\mathrm{d}}$, an auxiliary system, inspired by Chen et al. (2011), is designed as

$$\dot{\boldsymbol{\mu}}_{i1}=\begin{cases}-k_5\boldsymbol{\mu}_{i1}-\boldsymbol{\mu}_{i1}\left[\phi_i(\boldsymbol{\mu}_{i1}^{\mathrm{T}}\boldsymbol{\mu}_{i1})^{-1}\boldsymbol{E}_{i1}^{\mathrm{T}}\boldsymbol{\eta}_{i1}\boldsymbol{g}_{i1}\boldsymbol{\zeta}_{i1}\right.\\ \quad\left.+\dfrac{\boldsymbol{\zeta}_{i1}^{\mathrm{T}}\boldsymbol{\zeta}_{i1}}{2\boldsymbol{\mu}_{i1}^{\mathrm{T}}\boldsymbol{\mu}_{i1}}\right]+\boldsymbol{\zeta}_{i1}, & \boldsymbol{\mu}_{i1}^{\mathrm{T}}\boldsymbol{\mu}_{i1}\geq\mu_{i1\mathrm{b}},\\ \boldsymbol{0}, & \boldsymbol{\mu}_{i1}^{\mathrm{T}}\boldsymbol{\mu}_{i1}<\mu_{i1\mathrm{b}},\end{cases} \tag{36}$$

where $\boldsymbol{\mu}_{i1}=[\mu_{i11},\ \mu_{i12},\ \mu_{i13}]^{\mathrm{T}}$ and $\mu_{i1\mathrm{b}}$ is a positive constant to be determined by the designer.

Using the auxiliary system (36) and a similar analytical procedure to the one in Du et al. (2016), when $\boldsymbol{\mu}_{i1}^{\mathrm{T}}\boldsymbol{\mu}_{i1}\geq\mu_{i1\mathrm{b}}$, one has

$$\boldsymbol{\mu}_{i1}^{\mathrm{T}}\dot{\boldsymbol{\mu}}_{i1}\leq-k_5\boldsymbol{\mu}_{i1}^{\mathrm{T}}\boldsymbol{\mu}_{i1}-\phi_i\boldsymbol{E}_{i1}^{\mathrm{T}}\boldsymbol{\eta}_{i1}\boldsymbol{g}_{i1}\boldsymbol{\zeta}_{i1}+\frac{1}{2}\boldsymbol{\mu}_{i1}^{\mathrm{T}}\boldsymbol{\mu}_{i1}. \tag{37}$$

When $\boldsymbol{\mu}_{i1}^{\mathrm{T}}\boldsymbol{\mu}_{i1}<\mu_{i1\mathrm{b}}$, one has

$$\boldsymbol{\mu}_{i1}^{\mathrm{T}}\dot{\boldsymbol{\mu}}_{i1}=0. \tag{38}$$

By defining the angular rate tracking error as $\boldsymbol{e}_{i2}=\boldsymbol{x}_{i2}-\boldsymbol{x}_{i2\mathrm{d}}$ and using an RBFNN to approximate $\Gamma_2\boldsymbol{F}_{i2b}$ with Γ_2 being a positive parameter, the time derivative of $\boldsymbol{e}_{i2}$ is given by

$$\begin{aligned}\dot{\boldsymbol{e}}_{i2}=&\dot{\boldsymbol{x}}_{i2}-\dot{\boldsymbol{x}}_{i2\mathrm{d}}\\ =&\boldsymbol{F}_{i2b}+\boldsymbol{g}_{i2N}\boldsymbol{u}_{i0}+\boldsymbol{d}_i+\boldsymbol{\varepsilon}_i-\dot{\boldsymbol{x}}_{i2\mathrm{d}}\\ =&\Gamma_2^{-1}\boldsymbol{W}_{i2}^{*\mathrm{T}}\boldsymbol{\varphi}_{i2}+\boldsymbol{g}_{i2N}\boldsymbol{u}_{i0}+\boldsymbol{D}_{i2}-\dot{\boldsymbol{x}}_{i2\mathrm{d}},\end{aligned} \tag{39}$$

where $\boldsymbol{W}_{i2}^*$ is an optimal weight matrix, $\boldsymbol{\varphi}_{i2}$ is a Gaussian function vector, and $\boldsymbol{D}_{i2}=\Gamma_2^{-1}\boldsymbol{\xi}_{i2}+\boldsymbol{\varepsilon}_i+\boldsymbol{d}_i$ with $\boldsymbol{\xi}_{i2}$ being the RBFNN approximation error.

Assumption 3 For disturbance $\boldsymbol{D}_{i2}$, there exists an unknown positive constant $\bar{D}_{i2m}$ such that

$$\dot{\boldsymbol{D}}_{i2}^{\mathrm{T}}\dot{\boldsymbol{D}}_{i2}\leq\bar{D}_{i2m}. \tag{40}$$

The prediction error under the RBFNN and DO is constructed as

$$\begin{cases}\boldsymbol{\Upsilon}_{i2}=\boldsymbol{x}_{i2}-\hat{\boldsymbol{x}}_{i2},\\ \dot{\hat{\boldsymbol{x}}}_{i2}=\Gamma_2^{-1}\hat{\boldsymbol{W}}_{i2}^{*\mathrm{T}}\boldsymbol{\varphi}_{i2}+\boldsymbol{g}_{i2N}\boldsymbol{u}_{i0}+\hat{\boldsymbol{D}}_{i2}+k_8\boldsymbol{\Upsilon}_{i2},\end{cases} \tag{41}$$

where $\hat{\boldsymbol{W}}_{i2}^*$ and $\hat{\boldsymbol{D}}_{i2}$ are estimations of $\boldsymbol{W}_{i2}^*$ and $\boldsymbol{D}_{i2}$, respectively, and k_8 is a positive design parameter.

Then to estimate $\boldsymbol{D}_{i2}$, the DO is designed as

$$\begin{cases}\hat{\boldsymbol{D}}_{i2}=&\boldsymbol{\pi}_{i2}+k_9\boldsymbol{x}_{i2},\\ \dot{\boldsymbol{\pi}}_{i2}=&-k_9\boldsymbol{\pi}_{i2}-k_9\big[\Gamma_2^{-1}\hat{\boldsymbol{W}}_{i2}^{*\mathrm{T}}\boldsymbol{\varphi}_{i2}+\boldsymbol{g}_{i2N}\boldsymbol{u}_{i0}\\ &+k_9\boldsymbol{x}_{i2}-k_9^{-1}(k_{10}\boldsymbol{\Upsilon}_{i2}+\boldsymbol{e}_{i2})\big],\end{cases} \tag{42}$$

where k_9 and k_{10} are positive design parameters.

By taking the time derivative of Eq. (42), one has

$$\begin{aligned}\dot{\hat{\boldsymbol{D}}}_{i2}=&\dot{\boldsymbol{\pi}}_{i2}+k_9\dot{\boldsymbol{x}}_{i2}\\ =&k_9\tilde{\boldsymbol{D}}_{i2}+k_9\Gamma_2^{-1}\tilde{\boldsymbol{W}}_{i2}^{*\mathrm{T}}\boldsymbol{\varphi}_{i2}+k_{10}\boldsymbol{\Upsilon}_{i2}+\boldsymbol{e}_{i2},\end{aligned} \tag{43}$$

where $\tilde{\boldsymbol{W}}_{i2}^*=\boldsymbol{W}_{i2}^*-\hat{\boldsymbol{W}}_{i2}^*$ and $\tilde{\boldsymbol{D}}_{i2}=\boldsymbol{D}_{i2}-\hat{\boldsymbol{D}}_{i2}$ are estimation errors.

Taking the time derivative of $\tilde{\boldsymbol{D}}_{i2}$ yields

$$\dot{\tilde{\boldsymbol{D}}}_{i2}=\dot{\boldsymbol{D}}_{i2}-k_9\tilde{\boldsymbol{D}}-k_9\Gamma_2^{-1}\tilde{\boldsymbol{W}}_{i2}^{*\mathrm{T}}\boldsymbol{\varphi}_{i2}-k_{10}\boldsymbol{\Upsilon}_{i2}-\boldsymbol{e}_{i2}. \tag{44}$$

Design the control input signal and adaptive law as

$$\begin{aligned}\bar{\boldsymbol{u}}_{i0}=&\boldsymbol{g}_{i2N}^{-1}\big(-\Gamma_2^{-1}\hat{\boldsymbol{W}}_{i2}^{*\mathrm{T}}\boldsymbol{\varphi}_{i2}-\hat{\boldsymbol{D}}_{i2}+\dot{\boldsymbol{x}}_{i2\mathrm{d}}\\ &-\boldsymbol{K}_{11}\boldsymbol{e}_{i2}+k_{12}\boldsymbol{\mu}_{i2}-\phi_i\boldsymbol{g}_{i1}^{\mathrm{T}}\boldsymbol{\eta}_{i1}\boldsymbol{E}_{i1}\big),\end{aligned} \tag{45}$$

$$\dot{\hat{\boldsymbol{W}}}_{i2}^*=k_{13}\left[\boldsymbol{\varphi}_{i2}\Gamma_2^{-1}(\boldsymbol{e}_{i2}+k_{10}\boldsymbol{\Upsilon}_{i2})^{\mathrm{T}}-k_{14}\hat{\boldsymbol{W}}_{i2}^*\right], \tag{46}$$

where $\boldsymbol{K}_{11}$ is a diagonal matrix with positive elements, and k_{12}, k_{13}, and k_{14} are positive design parameters.

In practical engineering applications, actuators often encounter input saturation due to physical limitations, which is given by

$$\boldsymbol{u}_{i0}=\begin{cases}\boldsymbol{u}_{i0\max}, & \bar{\boldsymbol{u}}_{i0}\geq\boldsymbol{u}_{i0\max},\\ \bar{\boldsymbol{u}}_{i0}, & \boldsymbol{u}_{i0\min}<\bar{\boldsymbol{u}}_{i0}<\boldsymbol{u}_{i0\max},\\ \boldsymbol{u}_{i0\min}, & \bar{\boldsymbol{u}}_{i0}\leq\boldsymbol{u}_{i0\min},\end{cases} \tag{47}$$

where $\boldsymbol{u}_{i0\max}$ and $\boldsymbol{u}_{i0\min}$ are the maximum and minimum allowable values, respectively.

Inspired by Chen et al. (2011), to avoid persistent actuator saturation, the auxiliary system is introduced as

$$\dot{\boldsymbol{\mu}}_{i2}=\begin{cases}-k_{12}\boldsymbol{\mu}_{i2}-\boldsymbol{\mu}_{i2}\left[(\boldsymbol{\mu}_{i2}^{\mathrm{T}}\boldsymbol{\mu}_{i2})^{-1}\boldsymbol{e}_{i2}^{\mathrm{T}}\boldsymbol{g}_{i2N}\boldsymbol{\zeta}_{i2}\right.\\ \quad\left.+\dfrac{\boldsymbol{\mu}_{i2}^{\mathrm{T}}\boldsymbol{\mu}_{i2}}{2\boldsymbol{\zeta}_{i2}^{\mathrm{T}}\boldsymbol{\zeta}_{i2}}\right]+\boldsymbol{\zeta}_{i2}, & \boldsymbol{\mu}_{i2}^{\mathrm{T}}\boldsymbol{\mu}_{i2}\geq\mu_{i2\mathrm{b}},\\ 0, & \boldsymbol{\mu}_{i2}^{\mathrm{T}}\boldsymbol{\mu}_{i2}<\mu_{i2\mathrm{b}},\end{cases}\tag{48}$$

where $\boldsymbol{\mu}_{i2}=[\mu_{i21},\ \mu_{i22},\ \mu_{i23}]^{\mathrm{T}}$, $\mu_{i2\mathrm{b}}$ is a positive constant to be chosen by the designer, and $\boldsymbol{\zeta}_{i2}=\boldsymbol{u}_{i0}-\bar{\boldsymbol{u}}_{i0}$.

Using the auxiliary system (48) and a similar analytical procedure to the one in Du et al. (2016), regarding $\boldsymbol{\mu}_{i2}^{\mathrm{T}}\boldsymbol{\mu}_{i2}\geq\mu_{i2\mathrm{b}}$, one has

$$\boldsymbol{\mu}_{i2}^{\mathrm{T}}\dot{\boldsymbol{\mu}}_{i2}\leq-k_{12}\boldsymbol{\mu}_{i2}^{\mathrm{T}}\boldsymbol{\mu}_{i2}-\boldsymbol{e}_{i2}^{\mathrm{T}}\boldsymbol{g}_{i2N}\boldsymbol{\zeta}_{i2}+\frac{1}{2}\boldsymbol{\mu}_{i2}^{\mathrm{T}}\boldsymbol{\mu}_{i2}.\tag{49}$$

When $\boldsymbol{\mu}_{i2}^{\mathrm{T}}\boldsymbol{\mu}_{i2}<\mu_{i2\mathrm{b}}$, one has

$$\boldsymbol{\mu}_{i2}^{\mathrm{T}}\dot{\boldsymbol{\mu}}_{i2}=0.\tag{50}$$

Remark 2 From the auxiliary system (36), it is observed that if the filter error $\boldsymbol{\zeta}_{i1}=\boldsymbol{0}$, one has $\dot{\boldsymbol{\mu}}_{i1}=-k_5\boldsymbol{\mu}_{i1}$, showing that $\boldsymbol{\mu}_{i1}$ converges into the set $\boldsymbol{\mu}_{i1}^{\mathrm{T}}\boldsymbol{\mu}_{i1}<\mu_{i1\mathrm{b}}$. When $\boldsymbol{\mu}_{i1}$ is in the set $\boldsymbol{\mu}_{i1}^{\mathrm{T}}\boldsymbol{\mu}_{i1}<\mu_{i1\mathrm{b}}$, one can reset $\boldsymbol{\mu}_{i1}$ to $\boldsymbol{\mu}_{i1}^{\mathrm{T}}\boldsymbol{\mu}_{i1}\geq\mu_{i1\mathrm{b}}$ if saturation occurs, i.e., $\boldsymbol{\zeta}_{i1}\neq\boldsymbol{0}$. Then the auxiliary system (36) will be reactivated to compensate for the error. Such a procedure can be used to handle the auxiliary system (48) if saturation occurs ($\boldsymbol{\zeta}_{i2}\neq\boldsymbol{0}$) when $\boldsymbol{\mu}_{i2}$ is in the set $\boldsymbol{\mu}_{i2}^{\mathrm{T}}\boldsymbol{\mu}_{i2}<\mu_{i2\mathrm{b}}$.

Remark 3 In the presented control scheme, the attitude synchronization tracking error (17) is first transformed into a new set (Eq. (20)) using a smooth and strictly increasing function $\Theta(\cdot)$. Then based on the transformed attitude error dynamics (26) and the angular rate tracking error dynamics (39), NNs with updating laws (34) and (46) and DOs (30) and (42) are integrated to approximate the unknown nonlinear functions due to the actuator faults and inherent nonlinearities in the UAVs. To enhance the approximation ability, the prediction errors (29) and (41) are introduced into the approximators. Using the auxiliary systems (36) and (48) to deal with the filter error $\boldsymbol{\zeta}_{i1}$ and the actuator saturation (47), respectively, and integrating the approximated nonlinear functions, the overall controller can be developed as Eqs. (33) and (45).

3.3 Stability analysis

Theorem 1 Considering a group of UAVs described by Eqs. (1)–(4) with Assumptions 1–3, if the control laws are chosen as Eqs. (33) and (45), the prediction errors are constructed as errors (29) and (41), the disturbance observers are designed as Eqs. (30) and (42), the adaptive laws are developed as laws (34) and (46), and the auxiliary systems are constructed as systems (36) and (48). Then the attitudes of all UAVs can track their attitude references in a synchronized behavior even in the presence of actuator fault model (10), the attitude synchronization tracking errors are strictly confined within the prescribed performance bounds (19), and all signals in the closed-loop system are bounded.

Proof Choose a Lyapunov function candidate as

$$L=\sum_{i=1}^{N}L_i=\sum_{i=1}^{N}\left(\sum_{j=1}^{5}L_{i1j}+\sum_{j=1}^{5}L_{i2j}\right),\tag{51}$$

where $L_{i11}=\frac{1}{2}\tilde{\boldsymbol{D}}_{i1}^{\mathrm{T}}\tilde{\boldsymbol{D}}_{i1}$, $L_{i12}=\frac{1}{2}\boldsymbol{E}_{i1}^{\mathrm{T}}\boldsymbol{E}_{i1}$, $L_{i13}=\frac{1}{2k_6}\mathrm{tr}(\tilde{\boldsymbol{W}}_{i1}^{*\mathrm{T}}\tilde{\boldsymbol{W}}_{i1}^{*})$, $L_{i14}=\frac{1}{2}k_3\phi_i\boldsymbol{\Upsilon}_{i1}^{\mathrm{T}}\boldsymbol{\Upsilon}_{i1}$, $L_{i15}=\frac{1}{2}\boldsymbol{\mu}_{i1}^{\mathrm{T}}\boldsymbol{\mu}_{i1}$, $L_{i21}=\frac{1}{2}\tilde{\boldsymbol{D}}_{i2}^{\mathrm{T}}\tilde{\boldsymbol{D}}_{i2}$, $L_{i22}=\frac{1}{2}\boldsymbol{e}_{i2}^{\mathrm{T}}\boldsymbol{e}_{i2}$, $L_{i23}=\frac{1}{2k_{13}}\mathrm{tr}(\tilde{\boldsymbol{W}}_{i2}^{*\mathrm{T}}\tilde{\boldsymbol{W}}_{i2}^{*})$, $L_{i24}=\frac{1}{2}k_{10}\boldsymbol{\Upsilon}_{i2}^{\mathrm{T}}\boldsymbol{\Upsilon}_{i2}$, $L_{i25}=\frac{1}{2}\boldsymbol{\mu}_{i2}^{\mathrm{T}}\boldsymbol{\mu}_{i2}$, and tr(.) is the trace of a matrix.

Taking the time derivative of L_{i11} along with Eq. (32) gives

$$\begin{aligned}\dot{L}_{i11}=&\tilde{\boldsymbol{D}}_{i1}^{\mathrm{T}}\dot{\boldsymbol{D}}_{i1}-k_2\tilde{\boldsymbol{D}}_{i1}^{\mathrm{T}}\tilde{\boldsymbol{D}}_{i1}-k_2\Gamma_1^{-1}\tilde{\boldsymbol{D}}_{i1}^{\mathrm{T}}\tilde{\boldsymbol{W}}_{i1}^{*\mathrm{T}}\boldsymbol{\varphi}_{i1}\\&-k_3\phi_i\tilde{\boldsymbol{D}}_{i1}^{\mathrm{T}}\boldsymbol{\Upsilon}_{i1}-\tilde{\boldsymbol{D}}_{i1}^{\mathrm{T}}\boldsymbol{E}_{i1}-\phi_i\tilde{\boldsymbol{D}}_{i1}^{\mathrm{T}}\boldsymbol{\eta}_{i1}\boldsymbol{E}_{i1}.\end{aligned}\tag{52}$$

By substituting Eq. (33) into Eq. (27), one has

$$\begin{aligned}\dot{L}_{i12}=&\phi_i\Gamma_1^{-1}\boldsymbol{E}_{i1}^{\mathrm{T}}\boldsymbol{\eta}_{i1}\tilde{\boldsymbol{W}}_{i1}^{*\mathrm{T}}\boldsymbol{\varphi}_{i1}+\phi_i\boldsymbol{E}_{i1}^{\mathrm{T}}\boldsymbol{\eta}_{i1}\tilde{\boldsymbol{D}}_{i1}\\&-\boldsymbol{E}_{i1}^{\mathrm{T}}\boldsymbol{K}_4\boldsymbol{E}_{i1}+k_5\boldsymbol{E}_{i1}^{\mathrm{T}}\boldsymbol{\mu}_{i1}\\&+\phi_i\boldsymbol{E}_{i1}^{\mathrm{T}}\boldsymbol{\eta}_{i1}\boldsymbol{g}_{i1}\boldsymbol{\zeta}_{i1}+\phi_i\boldsymbol{E}_{i1}^{\mathrm{T}}\boldsymbol{\eta}_{i1}\boldsymbol{g}_{i1}\boldsymbol{e}_{i2}.\end{aligned}\tag{53}$$

In the view of the developed adaptive law (34), the time derivative of L_{i13} is given by

$$\begin{aligned}\dot{L}_{i13}=&-\phi_i\Gamma_1^{-1}\boldsymbol{E}_{i1}^{\mathrm{T}}\boldsymbol{\eta}_{i1}\tilde{\boldsymbol{W}}_{i1}^{*\mathrm{T}}\boldsymbol{\varphi}_{i1}\\&-\phi_i\Gamma_1^{-1}k_3\boldsymbol{\Upsilon}_{i1}^{\mathrm{T}}\tilde{\boldsymbol{W}}_{i1}^{*\mathrm{T}}\boldsymbol{\varphi}_{i1}\\&-k_7\mathrm{tr}(\tilde{\boldsymbol{W}}_{i1}^{*\mathrm{T}}\tilde{\boldsymbol{W}}_{i1}^{*})+k_7\mathrm{tr}(\tilde{\boldsymbol{W}}_{i1}^{*\mathrm{T}}\boldsymbol{W}_{i1}^{*}).\end{aligned}\tag{54}$$

By taking the time derivative of L_{i14}, one has

$$\begin{aligned}\dot{L}_{i14}=&k_3\phi_i\Gamma_1^{-1}\boldsymbol{\Upsilon}_{i1}^{\mathrm{T}}\tilde{\boldsymbol{W}}_{i1}^{*\mathrm{T}}\boldsymbol{\varphi}_{i1}+k_3\phi_i\boldsymbol{\Upsilon}_{i1}^{\mathrm{T}}\tilde{\boldsymbol{D}}_{i1}\\&-k_1k_3\phi_i\boldsymbol{\Upsilon}_{i1}^{\mathrm{T}}\boldsymbol{\Upsilon}_{i1}.\end{aligned}\tag{55}$$

Therefore, by considering Eqs. (52)–(55), the time derivative of $L_{i1}=\sum_{j=1}^{5}L_{i1j}$ satisfies

$$\begin{aligned}\dot{L}_{i1}\leq&\frac{\tilde{\boldsymbol{D}}_{i1}^{\mathrm{T}}\tilde{\boldsymbol{D}}_{i1}}{2h_{11}^2}+\frac{h_{11}^2\bar{D}_{i1m}}{2}-k_2\tilde{\boldsymbol{D}}_{i1}^{\mathrm{T}}\tilde{\boldsymbol{D}}_{i1}\\&+\frac{k_2\varGamma_1^{-1}\tilde{\boldsymbol{D}}_{i1}^{\mathrm{T}}\tilde{\boldsymbol{D}}_{i1}}{2h_{12}^2}+\frac{\tilde{\boldsymbol{D}}_{i1}^{\mathrm{T}}\tilde{\boldsymbol{D}}_{i1}}{2h_{13}^2}+\frac{h_{13}^2\boldsymbol{E}_{i1}^{\mathrm{T}}\boldsymbol{E}_{i1}}{2}\\&-\boldsymbol{E}_{i1}^{\mathrm{T}}\boldsymbol{K}_4\boldsymbol{E}_{i1}+\frac{k_2\varGamma_1^{-1}h_{12}^2\varphi_{i1m}}{2}\mathrm{tr}(\tilde{\boldsymbol{W}}_{i1}^{*\mathrm{T}}\tilde{\boldsymbol{W}}_{i1}^{*})\\&+k_5\boldsymbol{E}_{i1}^{\mathrm{T}}\boldsymbol{\mu}_{i1}+\phi_i\boldsymbol{E}_{i1}^{\mathrm{T}}\boldsymbol{\eta}_{i1}\boldsymbol{g}_{i1}\boldsymbol{\zeta}_{i1}+\phi_i\boldsymbol{E}_{i1}^{\mathrm{T}}\boldsymbol{\eta}_{i1}\boldsymbol{g}_{i1}\boldsymbol{e}_{i2}\\&-\frac{k_7}{2}\mathrm{tr}(\tilde{\boldsymbol{W}}_{i1}^{*\mathrm{T}}\tilde{\boldsymbol{W}}_{i1}^{*})+\frac{k_7}{2}\mathrm{tr}(\boldsymbol{W}_{i1}^{*\mathrm{T}}\boldsymbol{W}_{i1}^{*})\\&-k_1k_3\phi_i\boldsymbol{\varUpsilon}_{i1}^{\mathrm{T}}\boldsymbol{\varUpsilon}_{i1}+\boldsymbol{\mu}_{i1}^{\mathrm{T}}\dot{\boldsymbol{\mu}}_{i1},\end{aligned}\tag{56}$$

where

$$\begin{cases}\mathrm{tr}(\tilde{\boldsymbol{W}}_{i1}^{*\mathrm{T}}\boldsymbol{W}_{i1}^{*})\leq\dfrac{1}{2}\Big[\mathrm{tr}(\tilde{\boldsymbol{W}}_{i1}^{*\mathrm{T}}\tilde{\boldsymbol{W}}_{i1}^{\mathrm{T}})+\mathrm{tr}(\boldsymbol{W}_{i1}^{*\mathrm{T}}\boldsymbol{W}_{i1}^{*})\Big],\\ \tilde{\boldsymbol{D}}_{i1}^{\mathrm{T}}\dot{\boldsymbol{D}}_{i1}\leq\dfrac{1}{2}\Big(\dfrac{\tilde{\boldsymbol{D}}_{i1}^{\mathrm{T}}\tilde{\boldsymbol{D}}_{i1}}{h_{11}^2}+h_{11}^2\bar{D}_{i1m}\Big),\\ -\tilde{\boldsymbol{D}}_{i1}^{\mathrm{T}}\tilde{\boldsymbol{W}}_{i1}^{*\mathrm{T}}\boldsymbol{\varphi}_{i1}\leq\dfrac{1}{2}\Big[\dfrac{\tilde{\boldsymbol{D}}_{i1}^{\mathrm{T}}\tilde{\boldsymbol{D}}_{i1}}{h_{12}^2}+h_{12}^2\varphi_{i1m}\mathrm{tr}(\tilde{\boldsymbol{W}}_{i1}^{*\mathrm{T}}\tilde{\boldsymbol{W}}_{i1}^{*})\Big],\\ -\tilde{\boldsymbol{D}}_{i1}^{\mathrm{T}}\boldsymbol{E}_{i1}\leq\dfrac{1}{2}\Big(\dfrac{\tilde{\boldsymbol{D}}_{i1}^{\mathrm{T}}\tilde{\boldsymbol{D}}_{i1}}{h_{13}^2}+h_{13}^2\boldsymbol{E}_{i1}^{\mathrm{T}}\boldsymbol{E}_{i1}\Big),\end{cases}$$

where $||\boldsymbol{\varphi}_{i1}||^2\leq\varphi_{i1m}$, and h_{11}, h_{12}, and h_{13} are positive constants.

When $\boldsymbol{\mu}_{i1}^{\mathrm{T}}\boldsymbol{\mu}_{i1}\geq\mu_{i1\mathrm{b}}$, one has

$$\begin{aligned}\dot{L}_{i1}\leq&-\left(k_2-\frac{1}{2h_{11}^2}-\frac{k_2\varGamma_1^{-1}}{2h_{12}^2}-\frac{1}{2h_{13}^2}\right)\tilde{\boldsymbol{D}}_{i1}^{\mathrm{T}}\tilde{\boldsymbol{D}}_{i1}\\&-\left[\lambda_{\min}(\boldsymbol{K}_4)-\frac{h_{13}^2}{2}-\frac{k_5}{2}\right]\boldsymbol{E}_{i1}^{\mathrm{T}}\boldsymbol{E}_{i1}\\&+\phi_i\boldsymbol{E}_{i1}^{\mathrm{T}}\boldsymbol{\eta}_{i1}\boldsymbol{g}_{i1}\boldsymbol{e}_{i2}\\&-\frac{1}{2}\left(k_7-k_2\varGamma_1^{-1}h_{12}^2\varphi_{i1m}\right)\mathrm{tr}(\tilde{\boldsymbol{W}}_{i1}^{*\mathrm{T}}\tilde{\boldsymbol{W}}_{i1}^{*})\\&-k_1k_3\phi_i\boldsymbol{\varUpsilon}_{i1}^{\mathrm{T}}\boldsymbol{\varUpsilon}_{i1}-\frac{1}{2}\left(k_5-1\right)\boldsymbol{\mu}_{i1}^{\mathrm{T}}\boldsymbol{\mu}_{i1}\\&+\frac{k_7}{2}\mathrm{tr}(\boldsymbol{W}_{i1}^{*\mathrm{T}}\boldsymbol{W}_{i1}^{*})+\frac{h_{11}^2\bar{D}_{i1m}}{2}.\end{aligned}\tag{57}$$

When $\boldsymbol{\mu}_{i1}^{\mathrm{T}}\boldsymbol{\mu}_{i1}<\mu_{i1\mathrm{b}}$, one has

$$\begin{aligned}\dot{L}_{i1}\leq&-\left(k_2-\frac{1}{2h_{11}^2}-\frac{k_2\varGamma_1^{-1}}{2h_{12}^2}-\frac{1}{2h_{13}^2}\right)\tilde{\boldsymbol{D}}_{i1}^{\mathrm{T}}\tilde{\boldsymbol{D}}_{i1}\\&-\left[\lambda_{\min}(\boldsymbol{K}_4)-\frac{h_{13}^2}{2}-\frac{k_5}{2}-\frac{\phi_i}{2}\right]\boldsymbol{E}_{i1}^{\mathrm{T}}\boldsymbol{E}_{i1}\\&+\phi_i\boldsymbol{E}_{i1}^{\mathrm{T}}\boldsymbol{\eta}_{i1}\boldsymbol{g}_{i1}\boldsymbol{e}_{i2}\end{aligned}\tag{58}$$

$$\begin{aligned}&-\frac{1}{2}\left(k_7-k_2\varGamma_1^{-1}h_{12}^2\varphi_{i1m}\right)\mathrm{tr}(\tilde{\boldsymbol{W}}_{i1}^{*\mathrm{T}}\tilde{\boldsymbol{W}}_{i1}^{*})\\&-k_1k_3\phi_i\boldsymbol{\varUpsilon}_{i1}^{\mathrm{T}}\boldsymbol{\varUpsilon}_{i1}+\frac{k_7}{2}\mathrm{tr}(\boldsymbol{W}_{i1}^{*\mathrm{T}}\boldsymbol{W}_{i1}^{*})+\frac{h_{11}^2\bar{D}_{i1m}}{2}\\&+\frac{1}{2}\phi_i(\boldsymbol{\eta}_{i1}\boldsymbol{g}_{i1}\boldsymbol{\zeta}_{i1})^{\mathrm{T}}(\boldsymbol{\eta}_{i1}\boldsymbol{g}_{i1}\boldsymbol{\zeta}_{i1})+\frac{k_5}{2}\mu_{i1\mathrm{b}}.\end{aligned}$$

Similar to the analytical procedure in Du et al. (2016), synthesizing inequalities (57) and (58) yields

$$\begin{aligned}\dot{L}_{i1}\leq&-\left(k_2-\frac{1}{2h_{11}^2}-\frac{k_2\varGamma_1^{-1}}{2h_{12}^2}-\frac{1}{2h_{13}^2}\right)\tilde{\boldsymbol{D}}_{i1}^{\mathrm{T}}\tilde{\boldsymbol{D}}_{i1}\\&-\left[\lambda_{\min}(\boldsymbol{K}_4)-\frac{h_{13}^2}{2}-\frac{k_5}{2}-\frac{\phi_i}{2}\right]\boldsymbol{E}_{i1}^{\mathrm{T}}\boldsymbol{E}_{i1}\\&+\phi_i\boldsymbol{E}_{i1}^{\mathrm{T}}\boldsymbol{\eta}_{i1}\boldsymbol{g}_{i1}\boldsymbol{e}_{i2}\\&-\frac{1}{2}\left(k_7-k_2\varGamma_1^{-1}h_{12}^2\varphi_{i1m}\right)\mathrm{tr}(\tilde{\boldsymbol{W}}_{i1}^{*\mathrm{T}}\tilde{\boldsymbol{W}}_{i1}^{*})\\&-k_1k_3\phi_i\boldsymbol{\varUpsilon}_{i1}^{\mathrm{T}}\boldsymbol{\varUpsilon}_{i1}-\frac{1}{2}\left(k_5-1\right)\boldsymbol{\mu}_{i1}^{\mathrm{T}}\boldsymbol{\mu}_{i1}\\&+\frac{k_7}{2}\mathrm{tr}(\boldsymbol{W}_{i1}^{*\mathrm{T}}\boldsymbol{W}_{i1}^{*})+\frac{h_{11}^2\bar{D}_{i1m}}{2}\\&+\frac{1}{2}\phi_i(\boldsymbol{\eta}_{i1}\boldsymbol{g}_{i1}\boldsymbol{\zeta}_{i1})^{\mathrm{T}}(\boldsymbol{\eta}_{i1}\boldsymbol{g}_{i1}\boldsymbol{\zeta}_{i1})+\frac{k_5}{2}\mu_{i1\mathrm{b}}.\end{aligned}\tag{59}$$

Next, we will present the time derivatives of L_{i2j}, where $i\in\varOmega$ and $j=1,\ 2,...,\ 5$.

By recalling Eq. (44), the time derivative of L_{i21} is given by

$$\begin{aligned}\dot{L}_{i21}=&\tilde{\boldsymbol{D}}_{i2}^{\mathrm{T}}\dot{\boldsymbol{D}}_{i2}-k_9\tilde{\boldsymbol{D}}_{i2}^{\mathrm{T}}\tilde{\boldsymbol{D}}_{i2}-k_{10}\tilde{\boldsymbol{D}}_{i2}^{\mathrm{T}}\boldsymbol{\varUpsilon}_{i2}\\&-\tilde{\boldsymbol{D}}_{i2}^{\mathrm{T}}\boldsymbol{e}_{i2}-k_9\varGamma_2^{-1}\tilde{\boldsymbol{D}}_{i2}^{\mathrm{T}}\tilde{\boldsymbol{W}}_{i2}^{*\mathrm{T}}\boldsymbol{\varphi}_{i2}.\end{aligned}\tag{60}$$

Taking the time derivative of L_{i22} yields

$$\begin{aligned}\dot{L}_{i22}=&\varGamma_2^{-1}\boldsymbol{e}_{i2}^{\mathrm{T}}\tilde{\boldsymbol{W}}_{i2}^{*\mathrm{T}}\boldsymbol{\varphi}_{i2}+\boldsymbol{e}_{i2}^{\mathrm{T}}\tilde{\boldsymbol{D}}_{i2}-\phi_i\boldsymbol{e}_{i2}^{\mathrm{T}}\boldsymbol{g}_{i1}^{\mathrm{T}}\boldsymbol{\eta}_{i1}\boldsymbol{E}_{i1}\\&-\boldsymbol{e}_{i2}^{\mathrm{T}}\boldsymbol{K}_{11}\boldsymbol{e}_{i2}+k_{12}\boldsymbol{e}_{i2}^{\mathrm{T}}\boldsymbol{\mu}_{i2}+\boldsymbol{e}_{i2}^{\mathrm{T}}\boldsymbol{g}_{i2N}\boldsymbol{\zeta}_{i2}.\end{aligned}\tag{61}$$

In the view of law (46), the time derivative of L_{i23} is calculated as

$$\begin{aligned}\dot{L}_{i23}=&-\varGamma_2^{-1}\boldsymbol{e}_{i2}^{\mathrm{T}}\tilde{\boldsymbol{W}}_{i2}^{*\mathrm{T}}\boldsymbol{\varphi}_{i2}-\varGamma_2^{-1}k_{10}\boldsymbol{\varUpsilon}_{i2}^{\mathrm{T}}\tilde{\boldsymbol{W}}_{i2}^{*\mathrm{T}}\boldsymbol{\varphi}_{i2}\\&-k_{14}\mathrm{tr}(\tilde{\boldsymbol{W}}_{i2}^{*\mathrm{T}}\tilde{\boldsymbol{W}}_{i2}^{*})+k_{14}\mathrm{tr}(\tilde{\boldsymbol{W}}_{i2}^{*\mathrm{T}}\boldsymbol{W}_{i2}^{*}).\end{aligned}\tag{62}$$

Taking the time derivative of L_{i24} yields

$$\begin{aligned}\dot{L}_{i24}=&k_{10}\varGamma_2^{-1}\boldsymbol{\varUpsilon}_{i2}^{\mathrm{T}}\tilde{\boldsymbol{W}}_{i2}^{*\mathrm{T}}\boldsymbol{\varphi}_{i2}+k_{10}\boldsymbol{\varUpsilon}_{i2}^{\mathrm{T}}\tilde{\boldsymbol{D}}_{i2}\\&-k_8k_{10}\boldsymbol{\varUpsilon}_{i2}^{\mathrm{T}}\boldsymbol{\varUpsilon}_{i2}.\end{aligned}\tag{63}$$

In the subsequent analysis, the following inequalities are used:

$$\begin{cases}\mathrm{tr}(\tilde{\boldsymbol{W}}_{i2}^{*\mathrm{T}}\boldsymbol{W}_{i2}^{*})\leq\dfrac{1}{2}\Big[\mathrm{tr}(\tilde{\boldsymbol{W}}_{i2}^{*\mathrm{T}}\tilde{\boldsymbol{W}}_{i2}^{*})+\mathrm{tr}(\boldsymbol{W}_{i2}^{*\mathrm{T}}\boldsymbol{W}_{i2}^{*})\Big],\\ \tilde{\boldsymbol{D}}_{i2}^{\mathrm{T}}\dot{\boldsymbol{D}}_{i2}\leq\dfrac{1}{2}\Big[\dfrac{\tilde{\boldsymbol{D}}_{i2}^{\mathrm{T}}\tilde{\boldsymbol{D}}_{i2}}{h_{21}^2}+h_{21}^2\bar{D}_{i2m}\Big],\\ -\tilde{\boldsymbol{D}}_{i2}^{\mathrm{T}}\tilde{\boldsymbol{W}}_{i2}^{*\mathrm{T}}\boldsymbol{\varphi}_{i2}\leq\dfrac{1}{2}\Big[\dfrac{\tilde{\boldsymbol{D}}_{i2}^{\mathrm{T}}\tilde{\boldsymbol{D}}_{i2}}{h_{22}^2}+h_{22}^2\varphi_{i2m}\mathrm{tr}(\tilde{\boldsymbol{W}}_{i2}^{*\mathrm{T}}\tilde{\boldsymbol{W}}_{i2}^{*})\Big],\end{cases}$$

where $||\boldsymbol{\varphi}_{i2}||^2 \leq \varphi_{i2m}$, and h_{21} and h_{22} are positive constants.

Using the inequalities mentioned above and taking the time derivative of $L_{i2} = \sum_{j=1}^{5} L_{i2j}$, one has

$$\begin{aligned}\dot{L}_{i2} \leq & \frac{\tilde{\boldsymbol{D}}_{i2}^{\mathrm{T}}\tilde{\boldsymbol{D}}_{i2}}{2h_{21}^2} + \frac{h_{21}^2\bar{D}_{i2m}}{2} - k_9\tilde{\boldsymbol{D}}_{i2}^{\mathrm{T}}\tilde{\boldsymbol{D}}_{i2} \\ & + \frac{k_9\Gamma_2^{-1}\tilde{\boldsymbol{D}}_{i2}^{\mathrm{T}}\tilde{\boldsymbol{D}}_{i2}}{2h_{22}^2} + \boldsymbol{e}_{i2}^{\mathrm{T}}\boldsymbol{g}_{i2N}\boldsymbol{\zeta}_{i2} - \boldsymbol{e}_{i2}^{\mathrm{T}}\boldsymbol{K}_{11}\boldsymbol{e}_{i2} \\ & + k_{12}\boldsymbol{e}_{i2}^{\mathrm{T}}\boldsymbol{\mu}_{i2} + \frac{k_9\Gamma_2^{-1}h_{22}^2\varphi_{i2m}}{2}\mathrm{tr}(\tilde{\boldsymbol{W}}_{i2}^{*\mathrm{T}}\tilde{\boldsymbol{W}}_{i2}^{*}) \\ & - \phi_i\boldsymbol{e}_{i2}^{\mathrm{T}}\boldsymbol{g}_{i1}^{\mathrm{T}}\boldsymbol{\eta}_{i1}\boldsymbol{E}_{i1} - \frac{k_{14}}{2}\mathrm{tr}(\tilde{\boldsymbol{W}}_{i2}^{*\mathrm{T}}\tilde{\boldsymbol{W}}_{i2}^{*}) \\ & + \frac{k_{14}}{2}\mathrm{tr}(\boldsymbol{W}_{i2}^{*\mathrm{T}}\boldsymbol{W}_{i2}^{*}) - k_8k_{10}\boldsymbol{\Upsilon}_{i2}^{\mathrm{T}}\boldsymbol{\Upsilon}_{i2} + \boldsymbol{\mu}_{i2}^{\mathrm{T}}\dot{\boldsymbol{\mu}}_{i2}.\end{aligned} \tag{64}$$

By recalling inequality (49) and Eq. (50) and taking the procedure similar to inequalities (57)–(59), one has

$$\begin{aligned}\dot{L}_{i2} \leq & -\left(k_9 - \frac{1}{2h_{21}^2} - \frac{k_9\Gamma_2^{-1}}{2h_{22}^2}\right)\tilde{\boldsymbol{D}}_{i2}^{\mathrm{T}}\tilde{\boldsymbol{D}}_{i2} \\ & - \left[\lambda_{\min}(\boldsymbol{K}_{11}) - \frac{k_{12}}{2} - \frac{1}{2}\right]\boldsymbol{e}_{i2}^{\mathrm{T}}\boldsymbol{e}_{i2} \\ & - \frac{1}{2}(k_{14} - h_{22}^2\varphi_{i2m}k_9\Gamma_2^{-1})\mathrm{tr}(\tilde{\boldsymbol{W}}_{i2}^{*\mathrm{T}}\tilde{\boldsymbol{W}}_{i2}^{*}) \\ & - \phi_i\boldsymbol{e}_{i2}^{\mathrm{T}}\boldsymbol{g}_{i1}^{\mathrm{T}}\boldsymbol{\eta}_{i1}\boldsymbol{E}_{i1} - k_8k_{10}\boldsymbol{\Upsilon}_{i2}^{\mathrm{T}}\boldsymbol{\Upsilon}_{i2} \\ & - \frac{(k_{12}-1)}{2}\boldsymbol{\mu}_{i2}^{\mathrm{T}}\boldsymbol{\mu}_{i2} + \frac{1}{2}(\boldsymbol{g}_{i2N}\boldsymbol{\zeta}_{i2})^{\mathrm{T}}(\boldsymbol{g}_{i2N}\boldsymbol{\zeta}_{i2}) \\ & + \frac{k_{12}}{2}\mu_{i2\mathrm{b}} + \frac{k_{14}}{2}\mathrm{tr}(\boldsymbol{W}_{i2}^{*\mathrm{T}}\boldsymbol{W}_{i2}^{*}) + \frac{h_{21}^2\bar{D}_{i2m}}{2}.\end{aligned} \tag{65}$$

By combining inequalities (59) and (65), the time derivative of L_i is given by

$$\dot{L}_i \leq -\ell_i L_i + \Psi_i, \tag{66}$$

where $\ell_i = \min\{2[k_2 - 1/(2h_{11}^2) - k_2\Gamma_1^{-1}/(2h_{12}^2) - 1/(2h_{13}^2)],\ 2[\lambda_{\min}(\boldsymbol{K}_4) - h_{13}^2/2 - k_5/2 - \phi_i/2],\ 2k_6(k_7/2 - k_2\Gamma_1^{-1}h_{12}^2\varphi_{i1m}/2),\ 2k_1,\ k_5 - 1,\ 2[k_9 - 1/(2h_{21}^2) - k_9\Gamma_2^{-1}/(2h_{22}^2)],\ 2[\lambda_{\min}(\boldsymbol{K}_{11}) - k_{12}/2 - 1/2],\ 2k_{13}(k_{14}/2 - h_{22}^2\varphi_{i2m}k_9\Gamma_2^{-1}/2),\ 2k_8,\ k_{12} - 1\}$, and $\Psi_i = \frac{1}{2}k_7\mathrm{tr}(\boldsymbol{W}_{i1}^{*\mathrm{T}}\boldsymbol{W}_{i1}^{*}) + \frac{1}{2}h_{11}^2\bar{D}_{i1m} + \frac{1}{2}k_5\mu_{i1\mathrm{b}} + \frac{1}{2}\phi_i(\boldsymbol{\eta}_{i1}\boldsymbol{g}_{i1}\boldsymbol{\zeta}_{i1})^{\mathrm{T}}(\boldsymbol{\eta}_{i1}\boldsymbol{g}_{i1}\boldsymbol{\zeta}_{i1}) + \frac{1}{2}k_{12}\mu_{i2\mathrm{b}} + \frac{1}{2}(\boldsymbol{g}_{i2N}\zeta_{i2})^{\mathrm{T}}\cdot(\boldsymbol{g}_{i2N}\zeta_{i2}) + \frac{1}{2}k_{14}\mathrm{tr}(\boldsymbol{W}_{i2}^{*\mathrm{T}}\boldsymbol{W}_{i2}^{*}) + \frac{1}{2}h_{21}^2\bar{D}_{i2m}$.

Taking the time derivative of Eq. (51) yields

$$\dot{L} \leq -lL + \Psi, \tag{67}$$

where $l = \min\{l_i\}$ $(i \in \Omega)$, and $\Psi = \sum_{k=1}^{N}\Psi_k$.

Furthermore, L can be calculated as

$$0 \leq L \leq \frac{\Psi}{l} + \left[L(0) - \frac{\Psi}{l}\right]\mathrm{e}^{-lt}. \tag{68}$$

From inequality (68), it is known that $L \to \frac{\Psi}{l}$ as $t \to \infty$. Therefore, it can be concluded that all signals in the Lyapunov function of Eq. (51) are uniformly ultimately bounded (UUB). According to Eq. (20), it can be seen that the synchronization tracking errors $\boldsymbol{e}_{i1}$ $(i \in \Omega)$ are confined within the prescribed bounds since the errors $\boldsymbol{E}_{i1}$ $(i \in \Omega)$ are UUB. By recalling Eq. (18), it is observed that the individual attitude tracking errors $\tilde{\boldsymbol{x}}_{i1}$ $(i \in \Omega)$ are also UUB.

4 Simulations

In this section, the effectiveness of the proposed control scheme is verified via numerical simulations on a network of four UAVs. The communication topology and the corresponding weights are illustrated in Fig. 1. In the simulations, the initial attitudes of all UAVs are chosen as $\mu_i(0) = 1.719°$, $\alpha_i(0) = 2.865°$, $\beta_i(0) = 1.719°$, and the initial angular rates $p_i(0) = q_i(0) = r_i(0) = 0$ deg/s, $i = 1,\ 2,\ 3,\ 4$.

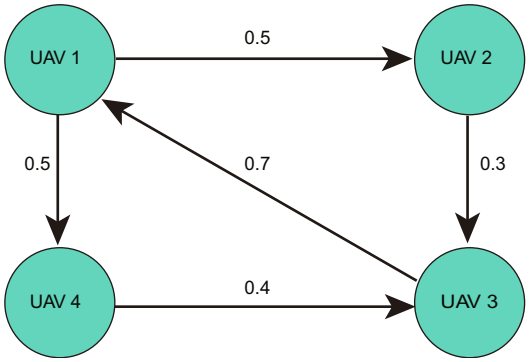

Fig. 1 Communication topology

In the simulations, the sideslip angle commands of four UAVs are chosen as 0°. The bank angle $\mu_{i\mathrm{d}}$ and angle of attack references $\alpha_{i\mathrm{d}}$ can be obtained by shaping the bank angle command $\mu_{i\mathrm{c}}$ and the angle of attack command $\alpha_{i\mathrm{c}}$ $(i = 1,\ 2,\ 3,\ 4)$, respectively, with a second-order linear command filter. The bank angle and angle of attack commands are chosen as

$$\begin{cases}\mu_{i\mathrm{c}} = 0°,\ \alpha_{i\mathrm{c}} = 2°, & 0\ \mathrm{s} \leq t < 6\ \mathrm{s}, \\ \mu_{i\mathrm{c}} = 10°,\ \alpha_{i\mathrm{c}} = 5°, & 6\ \mathrm{s} \leq t \leq 20\ \mathrm{s},\end{cases} \tag{69}$$

where $i = 1, 2, 3, 4$. The second-order filter is chosen as

$$\frac{\mu_{id}}{\mu_{ic}} = \frac{\alpha_{id}}{\alpha_{ic}} = \frac{\omega_d^2}{s^2 + 2\xi_d\omega_d s + \omega_d^2}, \tag{70}$$

where $\omega_d = 0.8$ and $\xi_d = 0.9$.

The upper and lower limits of input saturation are assumed to be $\boldsymbol{u}_{i0\max} = [60°, 60°, 60°]^T$ and $\boldsymbol{u}_{i0\min} = [-60°, -60°, -60°]^T$, respectively. To verify the fault-tolerant capability of the proposed control scheme, it is assumed that UAV 1, UAV 2, and UAV 3 encounter aileron, elevator, and rudder actuator faults at the 3rd, 8th, and 12th s, respectively. Based on the fault model (10), the following faults are adopted in the simulation:

1. UAV 1 aileron fault (t=3 s):

$$\begin{cases} \rho_{11} = 1,\ u_{1f1} = 0°, & 0\text{ s} \le t < 3\text{ s}, \\ \rho_{11} = 0.7,\ u_{1f1} = 17.19°, & 3\text{ s} \le t \le 20\text{ s}. \end{cases} \tag{71}$$

2. UAV 2 elevator fault (t=8 s):

$$\begin{cases} \rho_{22} = 1,\ u_{2f2} = 0°, & 0\text{ s} \le t < 8\text{ s}, \\ \rho_{22} = 0.7,\ u_{2f2} = 8.595°, & 8\text{ s} \le t \le 20\text{ s}. \end{cases} \tag{72}$$

3. UAV 3 rudder fault (t=12 s):

$$\begin{cases} \rho_{33} = 1,\ u_{3f3} = 0°, & 0\text{ s} \le t < 12\text{ s}, \\ \rho_{33} = 0.5,\ u_{3f3} = 17.19°, & 12\text{ s} \le t \le 20\text{ s}. \end{cases} \tag{73}$$

The design parameters are chosen as follows: $\lambda_1 = 2$, $\lambda_2 = 1.5$, $\underline{k}_{i1\nu} = 1$, $\varepsilon_{i1\nu 0} = 22.92°$, $\varepsilon_{i1\nu\infty} = 8.595°$, $\iota_{i1\nu} = 0.3$, $k_1 = 2$, $k_2 = 50$, $k_3 = 5$, $\boldsymbol{K}_4 = \mathrm{diag}(4, 12, 3.87)$, $k_5 = 1.5$, $k_6 = 30$, $k_7 = 0.02$, $\tau_i = 0.05$, $k_8 = 3$, $k_9 = 3$, $k_{10} = 4$, $\boldsymbol{K}_{11} = \mathrm{diag}(15.7, 8, 7)$, $k_{12} = 4$, $k_{13} = 30$, $k_{14} = 0.15$, $\Gamma_1 = 3$, and $\Gamma_2 = 2$. The Gaussian function in Zhang et al. (2017) is used in the RBFNN with the width of each neural cell being 20. The RBFNN in Eq. (27) contains 30 nodes for α_i, β_i, μ_i, and V_i with their centers evenly spaced in $[-28.65°, 28.65°] \times [-28.65°, 28.65°] \times [-28.65°, 28.65°] \times [20\text{ m/s}, 50\text{ m/s}]$. The RBFNN in Eq. (39) contains 30 nodes for V_i, α_i, β_i, p_i, q_i, r_i, δ_{ia0f}, δ_{ie0f}, and δ_{ir0f} with their centers evenly spaced in $[20\text{ m/s}, 50\text{ m/s}] \times [-28.65°, 28.65°] \times [-28.65°, 28.65°] \times [-57.3°, 57.3°] \times [-57.3°, 57.3°] \times [-57.3°, 57.3°] \times [-57.3°, 57.3°] \times [-57.3°, 57.3°] \times [-57.3°, 57.3°]$.

From Fig. 2, it is observed that the bank angles, angles of attack, and sideslip angles of UAVs 1–4 can successfully track the bank angle μ_{id}, angle of attack α_{id}, and sideslip angle references β_{id}, respectively, even when UAV 1 encounters an aileron fault at t=3 s, UAV 2 encounters an elevator fault at t=8 s, and UAV 3 confronts a rudder fault at t=12 s.

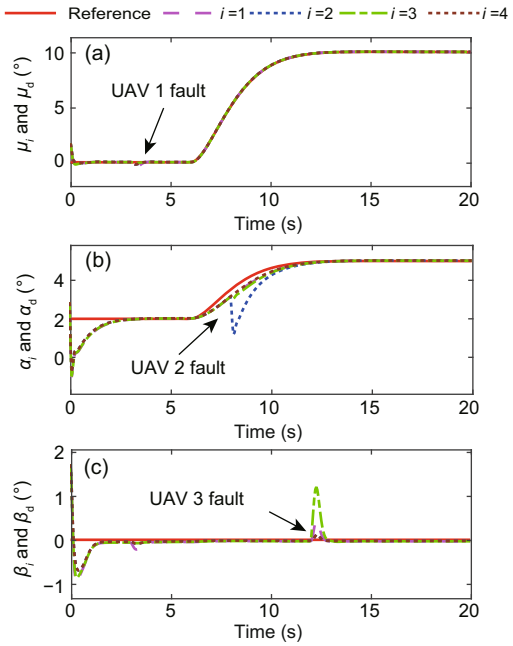

Fig. 2 Bank angles μ_i (a), angles of attack α_i (b), and sideslip angles β_i (c) of four UAVs, $i = 1, 2, 3, 4$

References to color refer to the online version of this figure

Fig. 3 shows the attitude tracking errors of four UAVs with respect to their individual attitude references (μ_{id}, α_{id}, and β_{id} for $i = 1, 2, 3, 4$). It can be seen that a slightly worse transient performance is induced when the aileron of UAV 1 is subjected to an actuator fault at t=3 s, the elevator of UAV 2 encounters an actuator fault at t=8 s, and the rudder of UAV 3 is subjected to an actuator fault at t=12 s. Moreover, it can be observed that the bank angle tracking errors of UAVs 2–4, the angle of attack tracking errors of UAVs 1, 3, and 4, and the sideslip angle tracking errors of UAVs 1, 2, and 4 encounter very slight performance degradations at t= 3, 8, and 12 s, respectively. This is due to the fact that in the communication network of numerous UAVs, the state variations of faulty UAVs can be sent to other healthy UAVs. Large performance degradations or instability can be caused if prompt actions are not adopted. Fortunately, under the proposed decentralized fault-tolerant cooperative control scheme, tracking errors are driven into regions containing zero in a timely

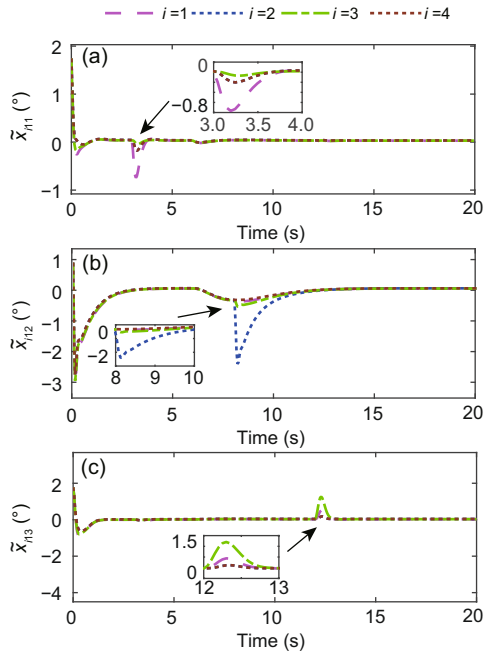

Fig. 3 Bank angles $\tilde{x}_{i11}$ (a), angles of attack $\tilde{x}_{i12}$ (b), and sideslip angles $\tilde{x}_{i13}$ (c) tracking errors of four UAVs with respect to their attitude references, $i = 1, 2, 3, 4$

References to color refer to the online version of this figure

manner, and the stability of the overall multi-UAV system is hence guaranteed.

The attitude synchronization tracking errors are shown in Fig. 4. It can be observed that the bank angle, angle of attack, and sideslip angle synchronization tracking errors strictly evolve in the region between the prescribed upper boundary of $\overline{k}_{i1\nu}\varepsilon_{i1\nu}$ and lower boundary of $-\underline{k}_{i1\nu}\varepsilon_{i1\nu}$, even in the presence of actuator faults.

The curves of control inputs are shown in Fig. 5. To attenuate the adverse effects of aileron, elevator, and rudder faults on the tracking performance, the control inputs are adjusted to achieve a satisfactory tracking performance, which are illustrated in Figs. 2–4. It can be seen that both aileron control input of UAV 1 and rudder control input of UAV 3 get saturated at the beginning. By imposing the saturation limits (47) on the control input signal (45), the control input signals sent to the UAV system are strictly restricted between $\boldsymbol{u}_{i0\min}$ and $\boldsymbol{u}_{i0\max}$. To compensate for the error between the control input signal and saturated control input signal in the event of input saturation, an auxiliary dynamic system (48) is introduced to pull the saturated control input signal back to the unsaturated region without

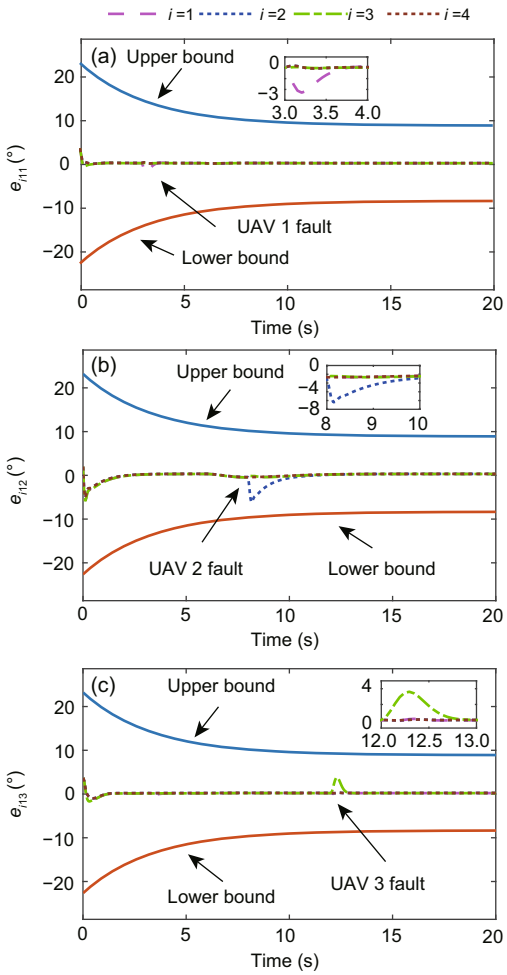

Fig. 4 Attitude synchronization tracking errors e_{i11} (a), e_{i12} (b), and e_{i13} (c) of four UAVs, $i = 1, 2, 3, 4$

References to color refer to the online version of this figure

persistent actuator saturation.

Figs. 6 and 7 illustrate the approximation errors under NNs and DOs. Fig. 6 shows that the nonlinear function $\boldsymbol{f}_{i1}$ in model (12) can be well approximated using error (29), Eq. (30), and law (34) even when aileron, elevator, and rudder faults are encountered by UAVs 1–3, respectively. Fig. 7 shows the approximation errors $\tilde{\boldsymbol{\Xi}}_i = [\tilde{\Xi}_{i1}, \tilde{\Xi}_{i2}, \tilde{\Xi}_{i3}]^{\mathrm{T}} = (\boldsymbol{F}_{i2} + \boldsymbol{d}_i) - (\Gamma_2^{-1}\hat{\boldsymbol{W}}_{i2}^{*}\boldsymbol{\varphi}_{i2} + \hat{\boldsymbol{D}}_{i2})$, which rapidly converge into the regions containing zero under prediction error (41), Eq. (42), and law (46). When UAVs 1–3 respectively encounter the aileron, elevator, and rudder faults, slightly degraded but acceptable approximation performances are induced. Under the proposed NNs and DOs, the approximation errors $\tilde{\Xi}_{i1}$, $\tilde{\Xi}_{i2}$, and $\tilde{\Xi}_{i3}$ are pulled into the small regions containing zero. Therefore, the approximation ability can be guaranteed. Furthermore,

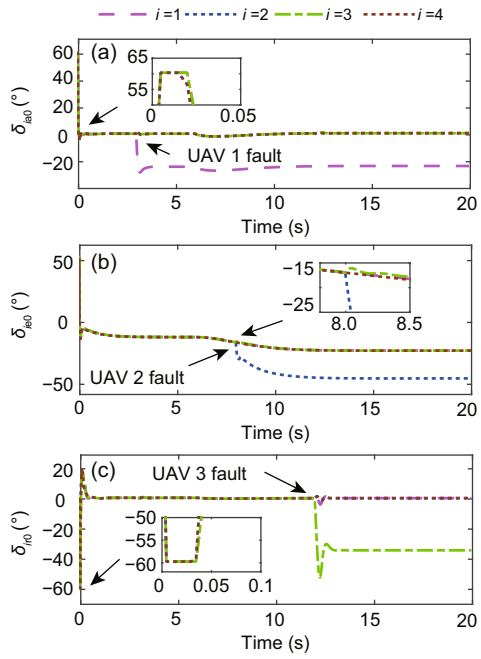

Fig. 5 Aileron (a), elevator (b), and rudder (c) control inputs of four UAVs, $i = 1, 2, 3, 4$

References to color refer to the online version of this figure

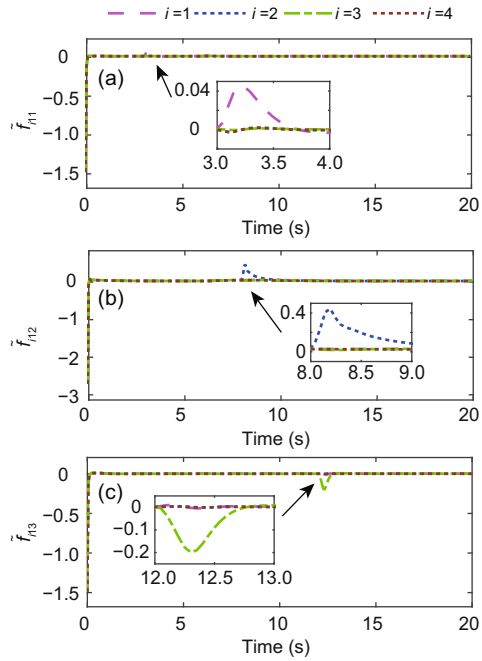

Fig. 6 Approximation errors of neural networks and disturbance observers under Eq. (30) and law (34): (a) $\tilde{f}_{i11}$; (b) $\tilde{f}_{i12}$; (c) $\tilde{f}_{i13}$

References to color refer to the online version of this figure

consider the simulation scenario in which UAVs 1–3 encounter aileron, elevator, and rudder faults, respectively, and UAV 4 is healthy. One can conclude that the proposed decentralized FTCC scheme with

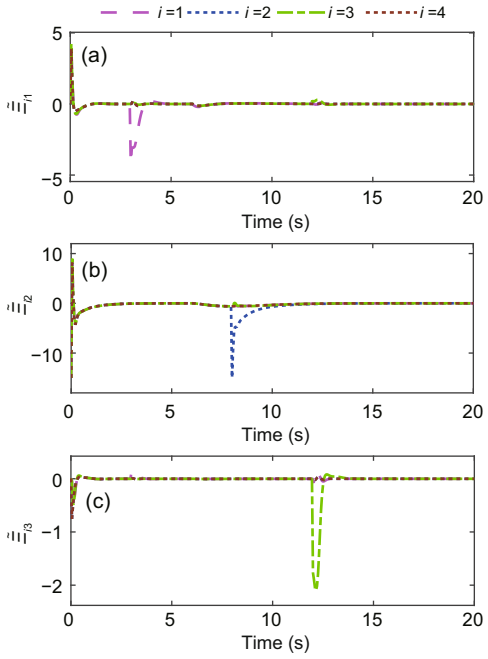

Fig. 7 Approximation errors of neural networks and disturbance observers under Eq. (42) and law (46): (a) $\tilde{\Xi}_{i1}$; (b) $\tilde{\Xi}_{i2}$; (c) $\tilde{\Xi}_{i3}$

References to color refer to the online version of this figure

the prescribed attitude synchronization tracking performance can be applied to UAVs in both faulty and healthy conditions.

5 Conclusions and future work

In this study, a decentralized fault-tolerant cooperative control scheme with the prescribed attitude synchronization tracking performance has been proposed for a group of UAVs in a directed communication network. Neural networks and disturbance observers were combined to approximate unknown nonlinear functions and nonlinear terms due to the actuator faults. Moreover, prediction errors were integrated into the adaptive laws and disturbance observers to enhance the approximation ability. By imposing the prescribed performance functions on the attitude synchronization errors, prescribed synchronization tracking control can be achieved. It has been theoretically proven that the proposed control scheme can make the attitudes of all UAVs synchronously track their attitude references. Simulation results of a network of four UAVs have demonstrated the effectiveness of the proposed control scheme.

Although the presented method can achieve

attitude synchronization tracking control with the prescribed performance in the presence of actuator faults and a fixed communication topology, issues of actuator dynamics and switching communication network have not been addressed in this study. Investigations of these factors in a decentralized fault-tolerant cooperative control framework can be parts of future work.

References

Bayezit I, Fidan B, 2013. Distributed cohesive motion control of flight vehicle formations. *IEEE Trans Ind Electron*, 60(12):5763-5772. https://doi.org/10.1109/TIE.2012.2235391

Bechlioulis CP, Rovithakis GA, 2008. Robust adaptive control of feedback linearizable MIMO nonlinear systems with prescribed performance. *IEEE Trans Autom Contr*, 53(9):2090-2099. https://doi.org/10.1109/TAC.2008.929402

Bechlioulis CP, Rovithakis GA, 2010. Prescribed performance adaptive control for multi-input multi-output affine in the control nonlinear systems. *IEEE Trans Autom Contr*, 55(5):1220-1226. https://doi.org/10.1109/TAC.2010.2042508

Chen M, Ge SS, Ren B, 2011. Adaptive tracking control of uncertain MIMO nonlinear systems with input constraints. *Automatica*, 47(3):452-465. https://doi.org/10.1016/j.automatica.2011.01.025

Du J, Hu X, Krstić M, et al., 2016. Robust dynamic positioning of ships with disturbances under input saturation. *Automatica*, 73:207-214. https://doi.org/10.1016/j.automatica.2016.06.020

Han Z, Lin Z, Fu M, et al., 2015. Distributed coordination in multi-agent systems: a graph Laplacian perspective. *Front Inform Technol Electron Eng*, 16(6):429-448. https://doi.org/10.1631/FITEE.1500118

He L, Sun X, Lin Y, 2016. Distributed output-feedback formation tracking control for unmanned aerial vehicles. *Int J Syst Sci*, 47(16):3919-3928. https://doi.org/10.1080/00207721.2016.1139758

Li Y, Wang C, Hu Q, 2017. Adaptive control with prescribed tracking performance for hypersonic flight vehicles in the presence of unknown elevator faults. *Int J Contr*, in press. https://doi.org/10.1080/00207179.2017.1406152

Liao F, Teo R, Wang JL, et al., 2017. Distributed formation and reconfiguration control of VTOL UAVs. *IEEE Trans Contr Syst Technol*, 25(1):270-277. https://doi.org/10.1109/TCST.2016.2547952

Lin W, 2014. Distributed UAV formation control using differential game approach. *Aerosp Sci Technol*, 35:54-62. https://doi.org/10.1016/j.ast.2014.02.004

Liu ZX, Yuan C, Zhang YM, et al., 2016. A learning-based fault tolerant tracking control of an unmanned quadrotor helicopter. *J Intell Robot Syst*, 84(1-4):145-162. https://doi.org/10.1007/s10846-015-0293-0

Liu ZX, Yuan C, Yu X, et al., 2017. Retrofit fault-tolerant tracking control design of an unmanned quadrotor helicopter considering actuator dynamics. *Int J Rob Nonl Contr*, in press. https://doi.org/10.1002/rnc.3889

Nigam N, Bieniawski S, Kroo I, et al., 2012. Control of multiple UAVs for persistent surveillance: algorithm and flight test results. *IEEE Trans Contr Syst Technol*, 20(5):1236-1251. https://doi.org/10.1109/TCST.2011.2167331

Qian M, Jiang B, Liu HHT, 2016. Dynamic surface active fault tolerant control design for the attitude control systems of UAV with actuator fault. *Int J Contr Autom Syst*, 14(3):723-732. https://doi.org/10.1007/s12555-015-0020-4

Ren W, Beard RW, Atkins EM, 2007. Information consensus in multivehicle cooperative control. *IEEE Contr Syst*, 27(2):71-82. https://doi.org/10.1109/mcs.2007.338264

Shi J, Yang Y, Sun J, et al., 2017. Fault-tolerant formation control of non-linear multi-vehicle systems with application to quadrotors. *IET Contr Theory Appl*, 11(17):3179-3190. https://doi.org/10.1049/iet-cta.2017.0569

Waharte S, Trigoni N, 2010. Supporting search and rescue operations with UAVs. Int Conf on Emerging Security Technologies, p.142-147. https://doi.org/10.1109/EST.2010.31

Wang B, Zhang Y, 2018. An adaptive fault-tolerant sliding mode control allocation scheme for multirotor helicopter subject to simultaneous actuator faults. *IEEE Trans Ind Electron*, 65(5):4227-4236. https://doi.org/10.1109/TIE.2017.2772153

Wu B, Wang D, Poh EK, 2011. Decentralized robust adaptive control for attitude synchronization under directed communication topology. *J Guid Contr Dynam*, 34(4):1276-1282. https://doi.org/10.2514/1.50189

Xu Q, Yang H, Jiang B, et al., 2014. Fault tolerant formations control of UAVs subject to permanent and intermittent faults. *J Intell Robot Syst*, 73(1-4):589-602. https://doi.org/10.1007/s10846-013-995

Xue R, Song J, Cai G, 2016. Distributed formation flight control of multi-UAV system with nonuniform time-delays and jointly connected topologies. *Proc Inst Mech Eng Part G: J Aerosp Eng*, 230(10):1871-1881. https://doi.org/10.1177/0954410015619446

Yan M, Zhu X, Zhang X, et al., 2017. Consensus-based three-dimensional multi-UAV formation control strategy with high precision. *Front Inform Technol Electron Eng*, 18(7):968-977. https://doi.org/10.1631/FITEE.1600004

Yu X, Liu ZX, Zhang YM, 2016. Fault-tolerant formation control of multiple UAVs in the presence of actuator faults. *Int J Rob Nonl Contr*, 26(12):2668-2685. https://doi.org/10.1002/rnc.3467

Yu X, Li P, Zhang YM, 2018a. The design of fixed-time observer and finite-time fault-tolerant control for hypersonic gliding vehicles. *IEEE Trans Ind Electron*, 65(5):4135-4144. https://doi.org/10.1109/TIE.2017.2772192

Yu X, Fu Y, Li P, et al., 2018b. Fault-tolerant aircraft control based on self-constructing fuzzy neural networks and multivariable SMC under actuator faults. *IEEE Trans Fuzzy Syst*, 26(4):2324-2335. https://doi.org/10.1109/TFUZZ.2017.2773422

Yu ZQ, Qu YH, Zhang YM, 2018. Safe control of trailing UAV in close formation flight against actuator fault and wake vortex effect. *Aerosp Sci Technol*, 77:189-205. https://doi.org/10.1016/j.ast.2018.01.028

Yuan C, Zhang YM, Liu ZX, 2015. A survey on technologies for automatic forest fire monitoring, detection, and fighting using unmanned aerial vehicles and remote sensing techniques. *Can J For Res*, 45(7):783-792. https://doi.org/10.1139/cjfr-2014-0347

Zhang G, Sun Z, Zhang W, et al., 2017. MLP-based adaptive neural control of nonlinear time-delay systems with the unknown hysteresis. *Int J Syst Sci*, 48(8):1682-1691. https://doi.org/10.1080/00207721.2017.1280555

Zhang YM, Jiang J, 2008. Bibliographical review on reconfigurable fault-tolerant control systems. *Ann Rev Contr*, 32(2):229-252. https://doi.org/10.1016/j.arcontrol.2008.03.008

Zou A, Hou Z, Tan M, 2008. Adaptive control of a class of nonlinear pure-feedback systems using fuzzy backstepping approach. *IEEE Trans Fuzzy Syst*, 16(4):886-897. https://doi.org/10.1109/TFUZZ.2008.917301